2022

Optimization of blast design for better fragmentation & reduction of ground vibration at Khao Mai Nuan pyrophyllite mine, Saraburi province, Thailand

Arif Khan
Faculty of Engineering

Optimization of Blast Design for Better Fragmentation & Reduction of Ground Vibration at Khao Mai Nuan Pyrophyllite Mine, Saraburi Province, Thailand

Mr. Arif Khan

A Thesis Submitted in Partial Fulfillment of the Requirements
for the Degree of Master of Engineering in Georesources and Petroleum Engineering
Department of Mining and Petroleum Engineering
FACULTY OF ENGINEERING
Chulalongkorn University
Academic Year 2022

การออกแบบงานระเบิดที่เหมาะสมเพื่อการแตกหักที่ดีขึ้นและลดการสั่นสะเทือนที่เหมืองไพโรฟิลไลต์ เขาไม้นวล จังหวัดสระบุรี ประเทศไทย

นายอาริฟ ข่าน

วิทยานิพนธ์นี้เป็นส่วนหนึ่งของการศึกษาตามหลักสูตรปริญญาวิศวกรรมศาสตรมหาบัณฑิต
สาขาวิชาวิศวกรรมทรัพยากรธรณีและปิโตรเลียม ภาควิชาวิศวกรรมเหมืองแร่และปิโตรเลียม
คณะวิศวกรรมศาสตร์ จุฬาลงกรณ์มหาวิทยาลัย
ปีการศึกษา 2565

Thesis Title	Optimization of Blast Design for Better Fragmentation & Reduction of Ground Vibration at Khao Mai Nuan Pyrophyllite Mine, Saraburi Province, Thailand
By	Mr. Arif Khan
Field of Study	Georesources and Petroleum Engineering
Thesis Advisor	Assistant Professor PIPAT LAOWATTANABANDIT, Ph.D.

Accepted by the FACULTY OF ENGINEERING, Chulalongkorn University in Partial Fulfillment of the Requirement for the Master of Engineering

..... Dean of the FACULTY OF ENGINEERING

(Professor SUPOT TEACHAVORASINSKUN, D.Eng.)

THESIS COMMITTEE

..... Chairman

(Associate Professor Pirat Jaroonpattanapong, Ph.D.)

..... Thesis Advisor

(Assistant Professor PIPAT LAOWATTANABANDIT, Ph.D.)

..... Examiner

(Assistant Professor RAPHAEL BISSEN, Ph.D.)

อาริฟ ข่าน : การออกแบบงานระเบิดที่เหมาะสมเพื่อการแตกหักที่ดีขึ้นและลดการสั่นสะเทือนที่เหมืองไพโรฟิลไลต์เขาไม้นวล จังหวัดสระบุรี ประเทศไทย. (Optimization of Blast Design for Better Fragmentation & Reduction of Ground Vibration at Khao Mai Nuan Pyrophyllite Mine, Saraburi Province, Thailand) อ.ที่ปรึกษาหลัก : ผศ.ดร.พิพัฒน์ เหล่าวัฒนบัณฑิต

การควบคุมการระเบิดให้มีการแตกหักที่ดีนั้น มีความสำคัญเป็นอย่างยิ่งในการลดผลกระทบต่อสิ่งแวดล้อมเนื่องมาจากการระเบิด รวมทั้งลดค่าใช้จ่ายในขั้นตอนของการทำเหมืองในลำดับถัดไป อันได้แก่ การตัก การขนส่ง การบดหยาบ และการบดละเอียด การออกแบบการระเบิดที่ดี ต้องอาศัยการปรับค่าตัวแปรต่างๆให้เหมาะสม ได้แก่ ระยะระหว่างแถว ระยะห่างระหว่างรูเจาะ ระยะอัดปิดปากรู ระยะเจาะต่ำกว่าพื้น และปริมาณวัตถุระเบิด ที่จะทำให้การระเบิดมีการแตกหักที่ต้องการ ด้วยค่าแรงสั่นสะเทือนภายใต้มาตรฐานที่กำหนดโดยหน่วยงานต่างๆ

การศึกษานี้เกี่ยวข้องกับการออกแบบตัวแปรในการระเบิด การแตกหัก และแรงสั่นสะเทือนจากการระเบิด ที่เหมืองแร่ไพโรฟิลไลต์ เขาไม้นวล จังหวัดสระบุรี ในขั้นตอนแรกของการศึกษาจะทำการเก็บตัวอย่างจากหน้างานที่มีการผลิตและทำการทดสอบค่าความแข็งแรง ส่วนประกอบ และคุณลักษณะของหินอื่นๆในห้องปฏิบัติการ คุณลักษณะทีได้ เช่น ชนิดของหิน การบรรยายตัวอย่างหิน ค่ากำลังอัดแกนเดียว ค่ากำลังแรงดึง และค่าความหนาแน่น จะถูกนำมาใช้ในการกำหนดค่าตัวแปรที่เหมาะสมและสร้างโมเดลคาดหมาย จากข้อมูลลักษณะหินและข้อมูลรูปร่างขนาดต่างๆ รูปแบบการระเบิดจำนวน 4 รูปแบบได้ถูกออกแบบเพื่อเสนอให้ไปทดลองในสนาม

ในการวิเคราะห์การกระจายขนาดของกองหินตกที่ได้จากการระเบิดแต่ละครั้ง จะอาศัยวิธีการแปลภาพถ่ายโดยซอฟท์แวร์ Image J โดยผลการกระจายขนาดเฉลี่ยจะถูกแสดงในรูปแบบของตารางและรูปภาพ ที่แสดงให้เห็นถึงประสิทธิภาพการแตกหักที่ดีขึ้น จากขนาดเฉลี่ย 25 นิ้ว ลดเหลือ 14 นิ้ว มีปริมาณหินก้อนโตน้อยลงมาก ในทางกลับกัน ได้มีการวัดค่าแรงสั่นสะเทือนที่เกิดจากการระเบิดในพื้นที่หน้างานโดยใช้เครื่องวัดยี่ห้อ Instantel Micromate เมื่อนำค่าระยะปรับทอนและค่าความเร็วสูงสุดของอนุภาคมาวิเคราะห์เชิงสถิติ พบว่าการสั่นสะเทือนที่เกิดจากการระเบิดอยู่ในระดับต่ำที่ไม่สามารถทำลายและส่งผลกระทบต่อสิ่งก่อสร้างรอบเหมืองได้ ค่าความเร็วสูงสุดของอนุภาคที่มากที่สุดคือ 1.65 มิลลิเมตรต่อวินาที และค่าความเร็วสูงสุดของอนุภาคที่น้อยที่สุดคือ 0.37 มิลลิเมตรต่อวินาที เพราะฉะนั้นจึงสามารถสรุปได้ว่าการออกแบบรูปแบบการระเบิดที่ได้ทำการทดสอบ มีความเหมาะสมต่อการผลิตแร่ที่ต้องการ ขนาดแตกหักที่ดีขึ้น อีกทั้งค่าความเร็วสูงสุดของอนุภาคก็ไม่ได้ส่งผลกระทบต่อโครงสร้างในพื้นที่ใกล้เคียงกับบริเวณเหมือง

สาขาวิชา	วิศวกรรมทรัพยากรธรณีและปิโตรเลียม	ลายมือชื่อนิสิต .....
ปีการศึกษา	2565	ลายมือชื่อ อ.ที่ปรึกษาหลัก .....

6372818421 : MAJOR GEORESOURCES AND PETROLEUM ENGINEERING
KEYWORD: SURFACE BLASTING / OPTIMIZATION / FRAGMENTATION / GROUND VIBRATION

Arif Khan : Optimization of Blast Design for Better Fragmentation & Reduction of Ground Vibration at Khao Mai Nuan Pyrophyllite Mine, Saraburi Province, Thailand. Advisor: Asst. Prof. PIPAT LAOWATTANABANDIT, Ph.D.

Control blasting with better fragmentation is very important to decrease the environmental impacts of blasting and the cost of downstream mining operations such as loading, transportation, crushing, and milling. Proper blasting designs with optimized parameters such as burden, spacing, stemming, sub-drilling, and amount of explosive ensure the required fragmentation with ground vibration within the standards set by different monitoring agencies.

This study dealt with the blasting design parameters, fragmentation, and ground vibration at the Khao Mai Nuan Pyrophyllite quarry Saraburi province, Thailand. First, grab samples were collected from the quarry's active benches and tested in a lab for strength, compositions and other rock characteristics. The obtained rock characteristic data such as rock type, rock description, uniaxial compressive strength (UCS), tensile strength, and density were used to optimize blast design parameters and build the predictive models. Based on the rock parameters data, four blast designs were proposed and then executed in the field.

A digital image processing method, image J software was employed for the size distribution analysis of each blast muckpile. The average size distribution results were obtained both in tabular and graphical form, which showed that the fragmentation performance had been increased from the average size of 25 inches to 14 inches with less noticeable boulder productions. On the other hand, blast-induced vibrations were measured carefully for all blasts conducted on-site using the Instantel Micromate seismograph device. Based on the statistical evaluation of the data pairs obtained from a scaled distance and peak particle velocity (PPV), the ground vibrations generated and propagated were very low to cause any kind of damage to any nearby structures within the vicinity of the mine. The highest peak particle velocity was recorded at 1.65 mm/s, and the lowest peak particle velocity (PPV) was 0.37 mm/s. Hence, it can be concluded that the proposed modified blast designs used for test blasts were suitable for the production of required size fragmentation, and it will be very unlikely that the PPV in such a range can affect any structure in the vicinity of the mine.

Field of Study:	Georesources and Petroleum Engineering	Student's Signature .....
Academic Year:	2022	Advisor's Signature .....

ACKNOWLEDGEMENTS

First of all, I would like to thank my advisor Dr. Pipat Laowattanabandit for providing an opportunity to work on this research topic. I am grateful for the time he spent helping, travelling, guiding and keeping me on track with this research work.

I would also like to thank Chulalongkorn University for providing me fully funded scholarship throughout my Master's degree.

I am truly grateful to the Mining and Petroleum Engineering department faculty for making me capable of doing this research work.

Special thanks to the committee members: Dr. Pirat Jaroonpattanapong and Dr. Raphael Bissen, for their cooperation, suggestions and assistance.

I sincerely thank Siam Cement Group (SCG) for allowing us to work at the Khao Mai Nuan Pyrophyllite quarry and supporting our research work.

Finally, I would like to thank my family for their support.

Arif Khan

TABLE OF CONTENTS

LIST OF TABLES

LIST OF FIGURES

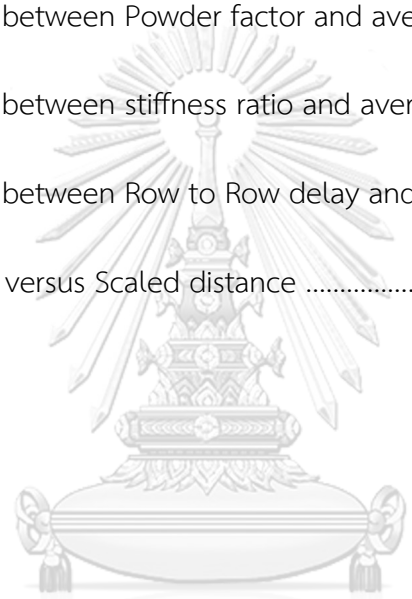

CHAPTER 1

INTRODUCTION

1.1 General Introduction

The most extensively used excavation technique for mining and civil engineering is blasting. Some improper blasts may induce ground vibration strong enough to damage and harm nearby lives and structures [1]. Therefore, the generation of ground shocks and their effects on the surrounding area have been gotten much attention. Several academics have proposed and identified several influenced factors, such as the percentage of charge utilized, the number of blast holes, the distance of the monitoring station from the blast face, geological and geotechnical characteristics of the host rock influencing ground vibration [2]. Hence, this topic of studies become very important in the 21st century to identify, monitor, and control the side effects of blasting, which directly affect the environment and disturb nearby humans, public properties, and artefacts.

The blasting method used in open-pit mines is to create fragmentation in rocks into the proper size. During the blast design phase, a method which results in the desired fragmentation has to be chosen because the degree of fragmentation has a significant impact on the cost of downstream mining operations, such as loading, transportation, crushing, and milling. Since blasting is the first stage of reducing rock size; therefore, the efficiency of downstream activities is determined by the distribution size of blasted rocks [3, 4]. Thus, it is clear that the drilling and blasting actions should be planned to achieve optimum fragmentation with low ground vibrations.

The parameters that influence propagation, the intensity of vibrations and fragmentation are characterized into two groups: controllable and uncontrollable parameters [5];

Controllable parameters are those that can be changed according to the requirements and needs. It depends on the allowable ground vibration limit and the required size of the fragmentation. Controllable parameters are subdivided into geometrical and explosive factors. The values of blast hole diameter, depth, drilling angle, sub-drill depth, bench height, stemming, burden, and spacing are called geometrical factors. However, charge weight, delay time, delay type, and type of explosive fall in the category of explosive factors [5]. Hence, better ground vibration and optimal fragmentation size can be achieved by controlling the controllable parameters.

The geotechnical-geological properties of the site, host rock characteristics, and the distance between blast structures are uncontrollable parameters; because no one on the site has any control over these parameters. Therefore, to match the site's conditions, the blasting engineer will change the blasting design to overcome the uncontrollable parameters [5].

1.2 Research Problem

Blasting is one of the most effective mining excavation methods as it permits maximum production with minimum cost. However, Pyrophyllite is not a common mineral, and the method of its extraction varies depending on the geology and characteristics of the rock mass. That is why conventional and traditional techniques of blasting practice at pyrophyllite quarries result in excess ground vibration and unwanted rock fragmentation (boulders) (Figure 1.1). Therefore, the optimization of various parameters (depth, drilling angle, sub drill depth, stemming, bench height, burden, and spacing) of blasting design will help to reduce the production of unwanted boulders or coarse fragmentation (which need secondary blasting) and decrease the ground vibrations below the approved peak particle velocity (PPV) limit set by the Department of Primary Industries and Mines (DPIM), Thailand.

Figure 1.1 Unwanted boulders after blasting at Pyrophyllite quarry

1.3 Scope and Objectives

This research aims to assess and optimize the controllable parameters (depth, drilling angle, sub-drill depth, bench height, stemming, burden, and spacing) at pyrophyllite quarry, which affects fragmentation and ground vibration. Since pyrophyllite is an uncommon mineral and the available research is inadequate, this study will have essential importance and contribution to the practice of blasting at pyrophyllite sites. In addition, it will guide the blaster or blasting engineer to conduct control blasts with better fragmentation and at the accepted rate of peak particle velocity (PPV). Furthermore, it will also help the company to limit the ground vibration within the quarry area in order to give safe environment to the surrounding new structures shown in Figure 1.2. Hence, the purpose of this study is to ascertain blasting design based on the optimized controllable parameters, which will lead the blasting operations towards better fragmentation size and approved ground vibrations level at at the Khao Mai Nuan Pyrophyllite quarry, Saraburi Province, Thailand.

The objectives are:

- To optimize blasting parameters (depth, drilling angle, sub drill depth, stemming, bench height, burden, and spacing).
- To control ground vibration.
- To achieve the required rock fragmentation.

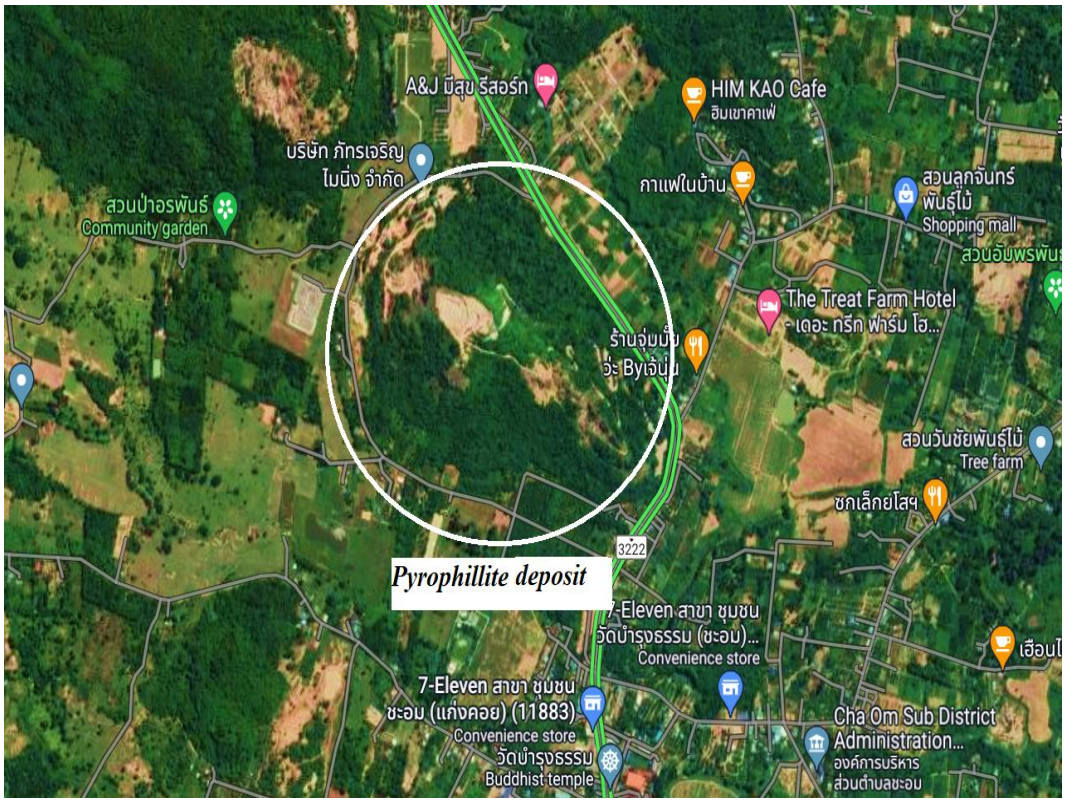

Figure 1.2 Buildings development near quarry (Google Earth-2022)

CHAPTER 2

LITERATURE REVIEWS

2.1 Bench Blasting Design Parameters

The primary objective of blasting is to provide a uniformly sized rock fragment, facilitating subsequent processing steps such as loading and crushing [6]. Several aspects, including the rock mass's mechanical qualities, the blast holes' geometry, the type and weight of explosives, the initiation system and pattern, and the delay times, all contribute to the final blast results [6, 7]. Figure 2.1 presents a quick glossary of the terms related to bench blasting geometry.

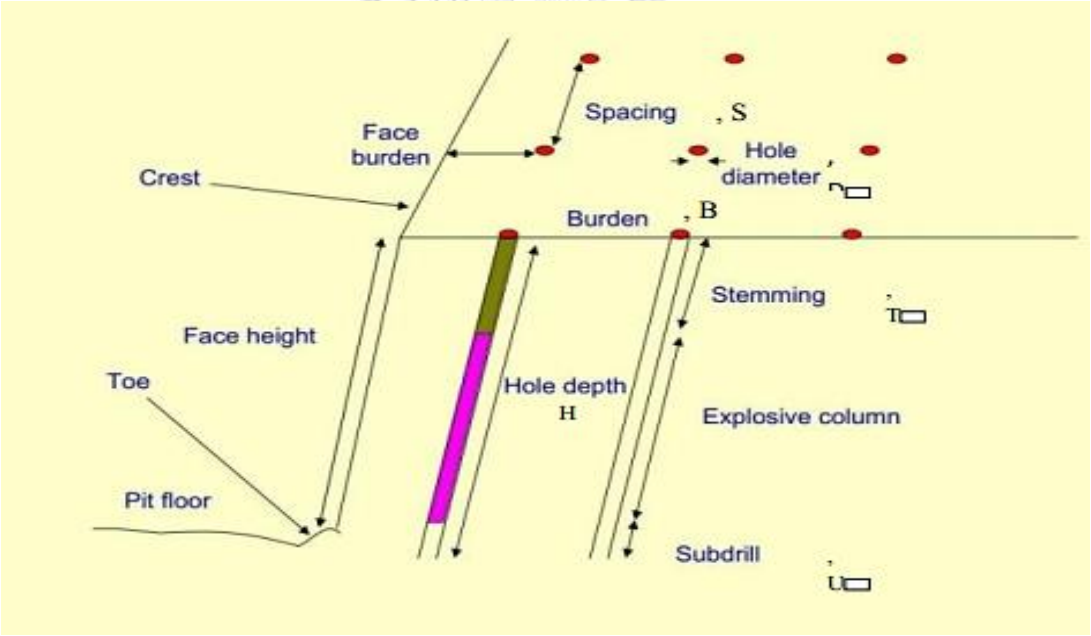

Figure 2.1 Bench blasting geometry

The parameters that influence propagation, the intensity of vibrations and fragmentation are characterized into two categories [4];

- Uncontrollable
- Controllable

2.2 Uncontrollable Parameters

The geological properties of the site, host rock geotechnical characteristics, and the distance between blasting site structures are considered as uncontrollable parameters; because no one in the site has any control over these parameters. Therefore, to match the conditions of the site; the blasting engineer will make changes in the blasting design to overcome the uncontrollable parameters.

2.2.1 Rock Geotechnical Properties

Optimal blasting results can be achieved if the impact of rock mass attributes on the blasting operations is understood. Multiple characteristics distinguish different types of rocks. Within relatively small areas, the composition and characteristics of the underlying rock mass change drastically [8]. This means that it is crucial to have a firm grasp on the dimensions of the rock mass to ensure an effective blast design.

2.2.1.1 Rock Strength

The strength of a rock is determined by force required to cause its failure. There are three different mechanisms by which rocks might fail: compression, tension, and shear [9]. Blast designs should put the rock under tension for breaking and in shear for creating smooth surfaces, such as presplitting, because the rock is often strongest in compression. Rocks are divided into several categories based on their compressive strength, as shown in Figure 2.2.

Grade	Classification	Field Identification	UCS (MPa)	Point load Index (MPa)	Example
R0	Extremely	Indented by thumb nail	<1	-	Stiff fault gouge
R1	Very weak	Peeled with a pocket knife	1 – 5	-	Highly weathered
R2	Weak	Peeled with a pocket knife with difficulty	5 – 25	-	Chalk
R3	Medium	Cannot be peeled with a pocket knife	25 – 50	1 – 2	Concreate
R4	Strong	Require more than one blow to fracture	50 – 100	2 – 4	Limestone
R5	Very strong	Require many blows to fracture	100 – 250	4 – 10	Amphibolite

Figure 2.2 Rock classifications by compressive strength [9, 10]

2.2.1.2 Elasticity

Elasticity is ability to resume its normal shape after being stretched. Young's modulus of elasticity and the coefficient of elasticity are common measures of elasticity.

The rock's stiffness and ability to resist external effects are best described by its modulus of elasticity. The explosive gasses pressure will have great difficulty compressing the rock if Young's modulus is high. Therefore, the explosive gas pressure must be lower than 5% of Young's modulus for effective blasting [11].

2.2.1.3 Density

The mass of a rock per unit volume is known as its density, and its specific gravity is the ratio of its density to that of water. Blasting engineers employ rock density to calculate the right energy or powder parameters. The rock's precise density is crucial for the blaster to convert rock volume into weight. Moreover, predicting the blast's yield is important for blast log.

In general, the rock's density helps determine how easy or difficult it is to break it. The density of the rock impacts the rock's energy propagation qualities and indicates the energy required to break and move the rock [12].

2.2.1.4 Porosity

The amount of air spaces within a rock is called its porosity. A rock with a high percentage of voids or pores spaces is considered extremely porous. The ability of a rock to absorb and store water is enhanced by the presence of such cavities or crevices. Vesicular basalt, known for its extreme porosity, has significantly reduced the need for explosion containment [12].

The effectiveness of blasting is also impacted by the degree of permeability of the rocks. Blasting highly porous rocks causes more energy loss and leads to more crushing and fines generation. Therefore, the high energy component of an explosive's total energy production does practically all of the work of fragmenting very permeable rock. The pore water pressure can significantly lower the compressive and shear strength of the porous rock [12]. Once these rocks become saturated, the effects of a blast are enhanced.

2.2.1.5 Rock Structure

In general, rocks are heterogeneous and anisotropic. Rock properties variation is crucial to blasting operations because it aids in forecasting the throw of fragmentation in the blasted material. The structural characteristics, such as faults, joints, bedding planes, cracks, fractures, and the formation's genesis, are typically the causes of the discrepancies [13]. Since the strength of the rock mass, its deformation characteristics, and the propagation of strain waves are all influenced by their nature, location, characteristics, and orientation, the impact of these structural features on how the rock mass responds to applied loads cannot be ignored during blast design.

Numerous scholars investigated how rock formations affected blasting and concluded that these structural characteristics impact blast outcomes more than explosive qualities and blast geometry [12, 13].

2.3 Controllable Parameters

Controllable parameters can be controlled according to the requirements and needs. It depends on the allowable ground vibration limit and the required size of the fragmentation. Controllable parameters are subdivided into geometrical and explosive factors. Geometrical parameters include blast hole diameter, depth, drilling angle, sub drill depth, bench height, stemming, burden, and spacing. However, the type and amount of explosive are considered explosive parameters.

2.3.1 Geometrical Parameters

2.3.1.1 Hole Diameter

The hole diameter selection is based on the required fragmentation average size for downstream operations such as loading, transportation, processing and to satisfy the production demands [14]. In a given blast, the distribution of explosives is greatly influenced by the diameter of the hole. Rocks with many joints benefit from small diameter holes. Large hole widths result in more productive drilling and blasting operations, reliable explosive detonation, higher shock energy, and cheaper drilling and blasting costs. The choice of hole diameter is influenced by the bench height, equipment available, required fragmentation size, explosive type, and rock geotechnical-geological properties. Blast hole diameter can be determined by using Equation 2.1 [5].

$$\textbf{Hole Diameter} = \frac{K}{5} \qquad \text{Equation (2.1)}$$

Where, K is the bench height

2.3.1.2 Sub-drill Depth

The portion of the blast hole bored below the planned grade elevation is known as sub-drilling. It is required to drill below the target grade to ensure that the blast will cause sufficient fragmentation at that level. The rock is most constricted at the bottom of the blasthole, making it the most difficult to break when the explosive is detonated; hence; hence sub-drilling is required. It is essential to sub-drill a blast hole to a depth of at least 0.3 to 0.5 times the maximum burden below the intended elevation to improve the amplitude of the tensile stress [14]. The depth of the sub-drilling will provide a smooth face for the preceding blast row, and the depth of the sub-drill will change with the type of rock.

2.3.1.3 Bench Height

Bench height is a key element in determining how a blast is designed. For most multi-level pits, the bench height, is typically rather constant, and its value is set to comply with the operational requirements of loading equipment [14]. The range of bench heights is quite large. Bench heights of 50 to 65 feet are typical in big open pits used for mining stone or minerals, while benches up to 100 feet tall have been seen on occasion. Bench heights are frequently restricted for safety reasons. In open pit metal mines, faces with heights between 30 and 60 feet have typically been regarded as the least expensive and risky to work on [15]. The thickness of ore or rock of a certain quality may determine the face height when selective mining or quarrying is required.

2.3.1.4 Stemming Height and Material

The upper length of the blast hole, which is often filled with an inert material to enclose the explosive gases, is known as the stemming height. Stemming main purpose is to contain the explosive's gas emissions until they have enough time to break apart and move the rock. The type of inert material and height of stemming have no appreciable impact on the properties of the blast-induced generated strain waves and do not enhance the influence of stress waves. Typically, the height of stemming is calculated by taking half to two-thirds of the maximum burden [14].

2.3.1.5 Burden

Burden is the distance between a front row blastholes and the closest free face. A line of previously fired holes from an earlier delay makes up the free face. The distance between rows, or rows in the typical scenario when rows are fired in sequence, is another way to define the burden [5]. Smaller-than-optimal burden causes fine fragmentation, high air blast levels, and a throw across a large distance. In addition to causing a serious back break, too much confinement of the explosives can result in strong ground vibrations and unwanted fragmentation [14]. Toe formation is another possible outcome. The burden has the least permitted error among all the blast design parameters. Equation 2.2 allows for the estimation of the burden [14].

$$B = 1.36\sqrt{i_b} \qquad \text{Equation (2.2)}$$

Where B is the burden, and i_b is the charge concentration.

2.3.1.6 Powder Factor

The relationship between total weights of explosives detonated in a blast and the volume of rock that is broken is known as the powder factor, which is also referred to as the blast or explosive factor in some contexts. The standard unit of measurement is pounds per cubic foot (lb/ft^3). When the burden stays constant, the average fragment size decreases as the powder factor in (lb/ft^3). rises [16]. The charging ratios may be as low as 0.15 to 0.25 kg/m^3 when blasting is limited to a single row of blast holes in soft laminated strata. The charge ratio in a jointed igneous rock can be as high as 0.6 kg/m^3, while they are typically about 0.45 kg/m^3 in tougher sedimentary layers. Equation 2.3 can be used to calculate the powder factor [16].

$$PF = \frac{W_t}{V} \qquad \text{Equation (2.3)}$$

Where, PF is powder factor (kg/m^3), W_t is total weight of explosive used in blast (kg) and V is volume of rock generated in blast.

2.3.1.7 Stiffness Ratio

Bench height of the blast divided by the blast's burden is the stiffness ratio. Assuming a constant bench height, the stiffness ratio improves as the blast burden decreases. What this means is that a higher stiffness ratio and better performance are achieved at smaller borehole diameters.

Stiffness ratio has its limits. A ratio greater than 4 does not result in economical cost or performance gains for blasts. Drill deviation increases with the length of the drill steel in relation to the diameter. Consequently, the performance is limited.

On the other hand, the load increases with the size of the drill steel. Due to poor performance, including an increase in oversize, this lowers the stiffness ratio. Therefore, when it comes to drilling and blasting, bigger is not necessarily better.

2.3.2 Type and Properties of Explosives

The kind and characteristics of the explosives employed significantly impact the output of a detonation. The characteristic of explosives influencing the blast result are density, detonation velocity, detonation pressure, water resistance, and explosive strength [14, 16].

If all other design parameters of the blast are the same, high dense explosive, energy, the velocity of detonation and detonation pressure will result in finer fragmentation. An explosive's sensitivity is influenced by its density. The explosive's sensitivity increases with decreasing density. Additionally, water-resistant explosives must be used when blast holes are wet to maintain their effectiveness. Due to environmental restrictions, explosives that emit fewer fumes and less hazardous fumes should be utilized, especially in mining operations near cities.

2.4 Delay Timing

It is extremely uncommon for a conventional blast to go off with all charges exploding simultaneously. Usually, there is a certain amount of time, along with a direction, for delaying the detonation.

Longer delay times are used for tunnels, drifts, and shafts without a free face parallel to the holes' axis. These are designed to provide the rock that has been shattered by the initial holes enough time to be ejected so that the rock blasted by the subsequent holes can expand [17]. Millisecond delays are utilized mostly between blast holes in surface mining and construction.

2.5 Initiation Patterns

Row delays cannot compete with V, V1, and V2 Patterns. These lead to better fragmentation due to decreased hole burden, improved spacing at the moment of hole initiation, and in-flight collisions of broke rock throughout its movement. As a result of the back-row's holes' delayed action, there is less back-break, which increases the bench wall stability [17, 18].

A pattern with holes drilled (staggered) in an equilateral triangular shape is the best one currently feasible. With this, there is a roughly 1.16 ratio between drilled spacing and burden. A V1 initiation sequence and holes drilled on an equilateral triangle grid have produced an effective spacing (S) to burden (B) ratio of approximately 3.5. The open-pit mining blasting patterns are shown in Figure 2.3 as V, V1, and V2.

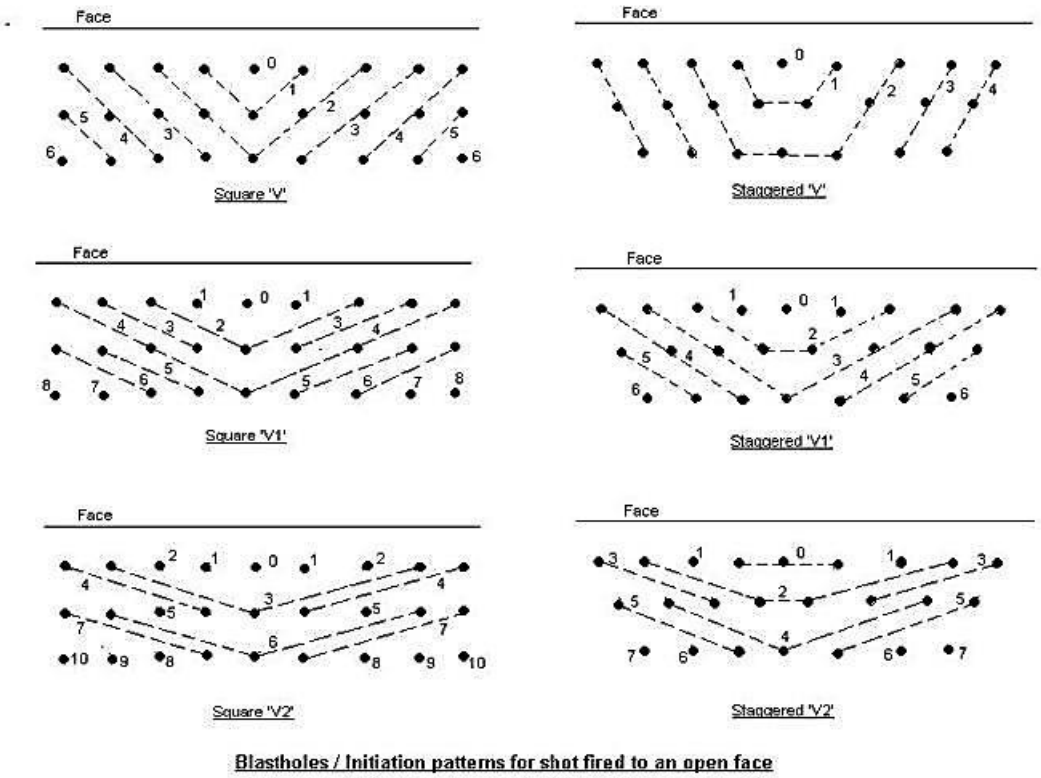

Figure 2.3 Blast holes initiation Patterns [14]

2.6 Theory of Blasting

Seismic movement in the ground is called Ground Vibrations. Some of the main operations responsible for the ground vibration are blasting, drilling, excavation, etc. Ground vibrations during blasting are a type of energy that travels through the near ground and may damage near property and structure when the vibration exceeds or reach the threshold limit [19]. The energy released in the form of seismic waves from a single hole during blasting spread in 360 degrees with different frequencies. The ground vibration limit depends on many factors (Figure 2.4);

- Weight of charge (Charge quantity)
- Constriction factor
- Host rock characteristics
- Buffer area of blasting site (Distance from blast hole)
- Geology of the site

Selection of optimal blasting method, accurate drilling and best firing pattern may control and limit ground vibration within the buffer zone (Lease area of the mine). Ground vibrations are different kind of seismic waves with different properties.

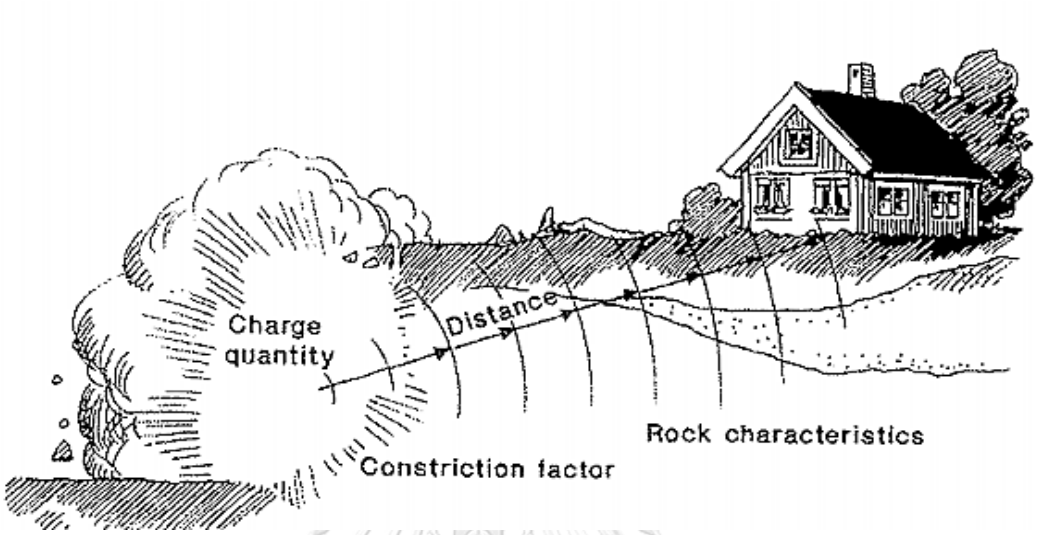

Figure 2.4 Show the visual representation of factors effecting ground vibration [19]

2.6.1 P-wave – Primary Wave

The wave that travels through the earth at the quickest speed is the compressional or P wave. Imagine a long steel rod that has been hammered on the end. This is the easiest way to understand how the particles in the P wave move. In other words, the wave's constituent particles move in the same direction as the wave's propagation as the compressive pulse moves along the rod [19, 20].

With velocities characteristic of the material it travels through, the P wave radiates forth from the blast hole in all directions. Figures 2.5 and 2.6 show how P waves move like waves.

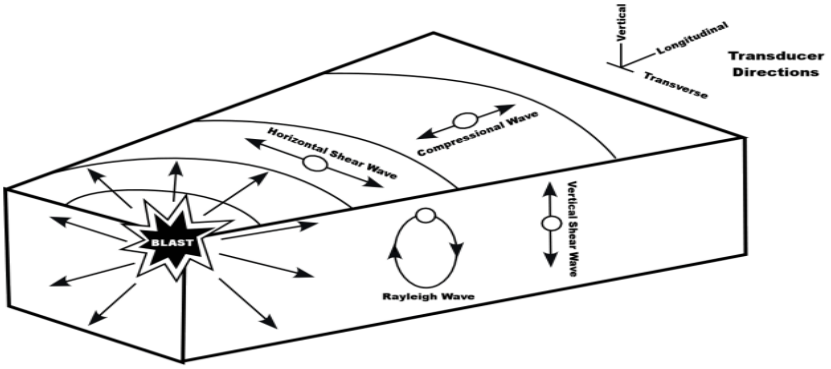

Figure 2.5 Motion of particle related to different waves [19]

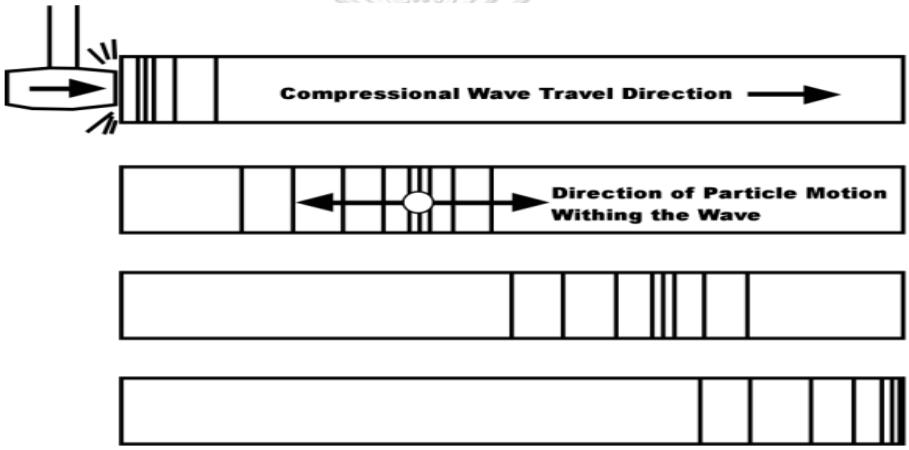

Figure 2.6 Particle motion in compressional (P) wave

2.6.2 S-wave – Secondary Wave

Velocity of the shear wave, also known as the S wave, is about equal to 50–60% that of the P wave. Shaking a rope at one end will show how the wave constituent particles move. The wave moves along the rope, but the wave's particles move perpendicular to the wave direction of motion [19]. Figures 2.5 and 2.7 show an illustration of the S wave motion. Because the P and S waves move through the rock's body in three dimensions, they are frequently called "body waves."

The speed of this wave is slower than P-wave but moves at the right angle to the propagation through the medium. The S-wave does not change the density, but it changes the shape of the materials [19, 20].

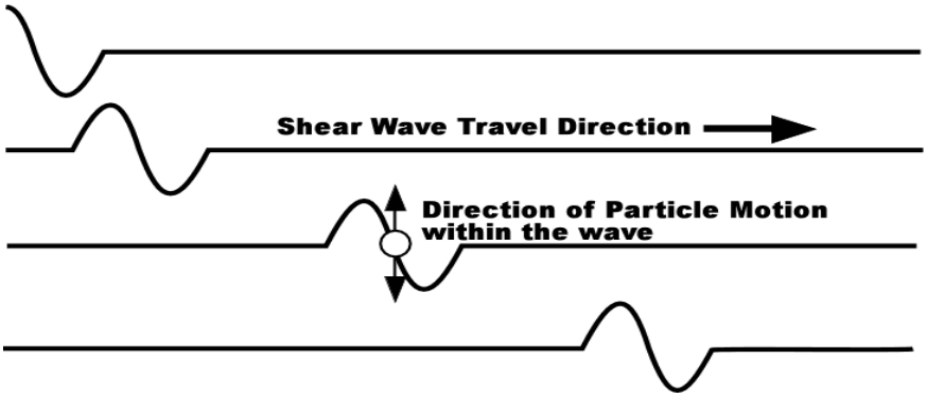

Figure 2.7 Shear (S) wave particle motion [19]

2.6.3 R-wave – Rayleigh Wave

The Rayleigh wave, often known as the R wave, is a surface wave that travels more slowly than the other two waves and rapidly declines with depth [19]. The wave constituent particles travel elliptically on a vertical plane parallel to its propagation path. The motion is counterclockwise to the wave motion at the surface. Figure 2.5 depicts how the R waves move as waves.

It is also called Surface wave and travel more slowly than S and P waves. The particle in R-wave move in the vertical plans and in the same direction of propagation.

In Figure 2.8, the key characteristics of the ground vibration that reaches a distant location are shown.

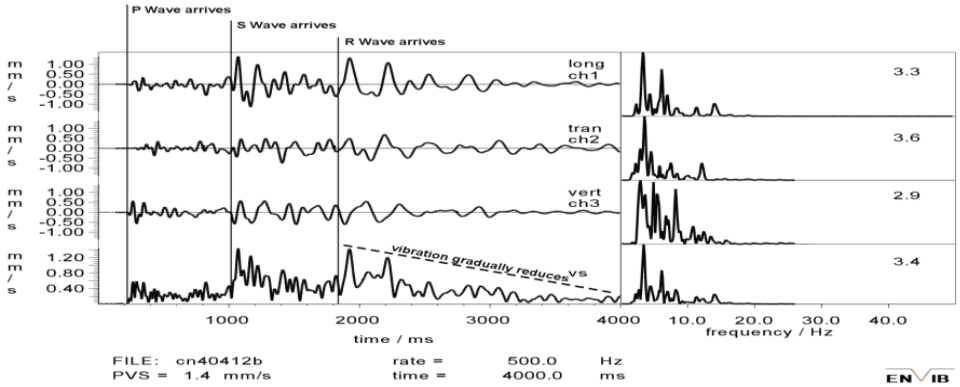

Figure 2.8 P, S and R wave trace from a single hole blast [21]

This shows the wave trail at a location around 1800 meters from a single hole blast of 1000 kg of explosives detonated in the overburden of a coal mine in the Hunter Valley. The P wave enters first, followed by the different P wave-related vibrations that are reflected and refracted [22]. This vibration progressively decreases until the S wave, and its accompanying reflected and refracted waves arrive 800 ms later. The R wave and its accompanying reflections and refractions arrive 900 ms later. After the 4-second time interval, the vibration eventually reaches zero again.

At this point, it is important to point out that the formation of the Shear and Rayleigh waves in Figure 2.8 was seen in locations with solid horizontal structures, such as coal overburden and basalt with horizontal clay layers [23]. Due to short distances and undetectable Rayleigh waves at most other sites, it could not distinguish between the Shear and Rayleigh waves by looking at the wave traces. Figure 2.9 depicts a typical wave trace to illustrate this.

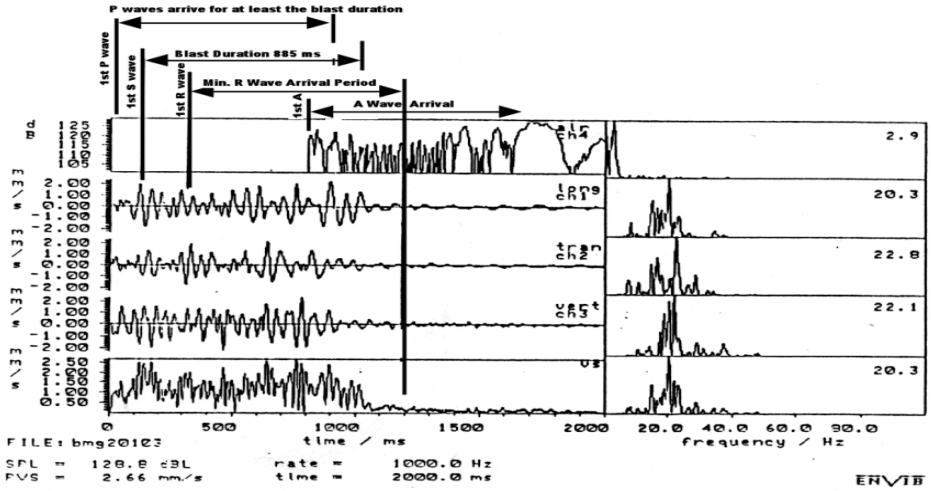

Figure 2.9 P, S and R Wave trace from a multi holes blast [21]

The wave trace for a rhyodacite quarry is displayed above. There were 108 holes shot in two rows, with an average charge mass of 127 kg. The distance to the monitoring station was 335 meters. Along with the projected arrival period of the P, S, and R waves, the 885 ms blast duration (the amount of time between the explosion of the first and final hole in the pattern) is shown Figure 2.9.

At locations without horizontal structures, the wave reflections and refractions that cause the vibrations that are so prominent in the first example likewise absent in areas free of horizontal structures.

Measurement of ground vibration can be done at one or more than one point at ground level. Particles velocities should be measured in vertical, longitudinal, and traverse directions for the complete analysis [24]. The vibration should be recorded as a function of time, and then measured the other parameters: displacement, particle velocity, and acceleration. These parameters are important and depend directly on the damage criterion for the structure. With known values of the mentioned parameters, the peak value can be easily calculated.

2.7 Zones of Explosion

During blasting, not all the energy produced by the explosion is used for the fragmentation of rock but 1-20% of the total energy travel around the site in the form of shock waves [19]. Which creates a vibration on the surface. However, researchers suggests that 5-15% of the total energy produced by explosive charge is propagated to the nearby structures and area as shock waves. The remaining explosive energy 75 -80 % is released as gaseous products of the reaction at extremely high pressures and temperatures. The destruction and deformation around the explosion are divided into three zones. They are;

- Shock zone
- Non-linear zone
- Elastic zone

The shockwave's radial compressive stresses overcome the surrounding rock's dynamic compressive strength in the first zone, causing crushing when the rock fails in compression, as seen in Figure 2.10 (A). The tangential stress causes fracture in the second zone, as seen in Figure 2.10 (B). Since the rock's tensile strength is low,

tangential tensile pressures result in cracks. The strain wave is reflected and may produce cracking when it reaches the free surface of the rock, as shown in Figure 2.8 (D).

As longitudinal waves have a greater velocity than shear waves and the strength of the rock in tension is significantly lower than in compression, the reflected wave will shatter the rock in tension if the tensile strength is exceeded. Nonetheless, high compressive tensions inside the rock continue to release as the burden advances, generating additional tensile stresses that finish the fragmentation process [19].

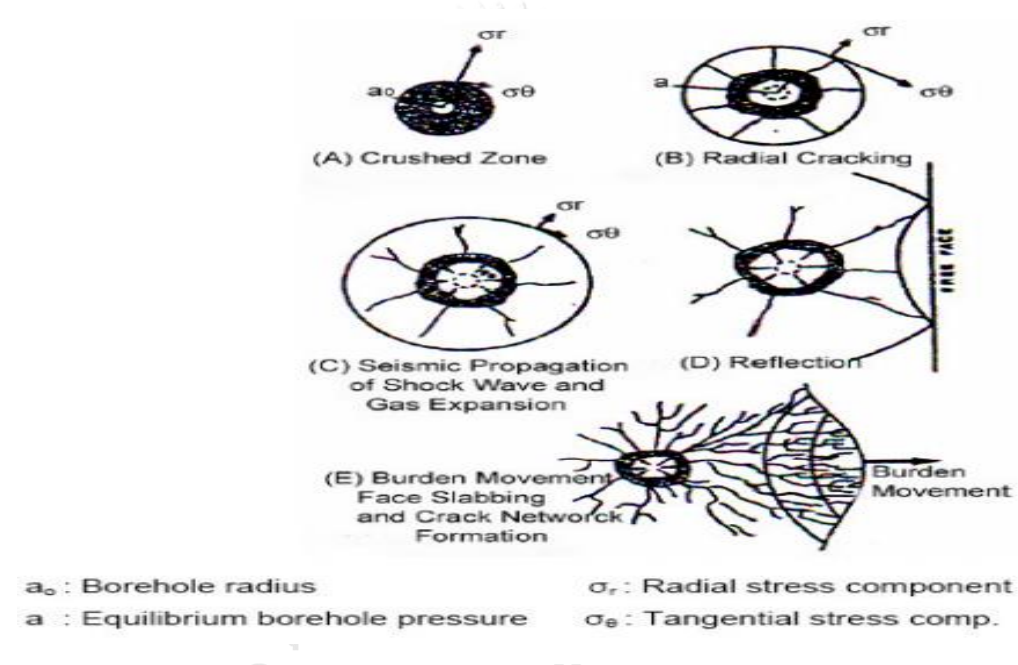

Figure 2.10 Events in the rock mass following the blasting [19]

2.8 The Nature of Ground Vibration

When the blasthole is detonated using explosive charge, the surrounding rock around explosive is cracked, shattered, and detached from the strata under the provided designs conditions. At a given distance from the blasthole, the explosive energy produced by the blast diminishes to a level that does not cause additional breaking (back-break) and continues to travel through the rock as an elastic ground vibration [25].

With increasing distance, the ground vibration radiates from the hole at a progressively lower intensity until it is barely perceptible. Structures will be damaged by ground vibration at high enough levels, although individuals within buildings may experience panic at levels considerably below those that cause structural damage [19].

One may demonstrate how the energy moves as waves by dropping a stone into a still body of water. Waves that radiate concentrically out from the center are created close to the point where the stone descends. As seen in Figure 2.11, the waves amplitude is highest near the drop point and gradually drops as they propagate outward.

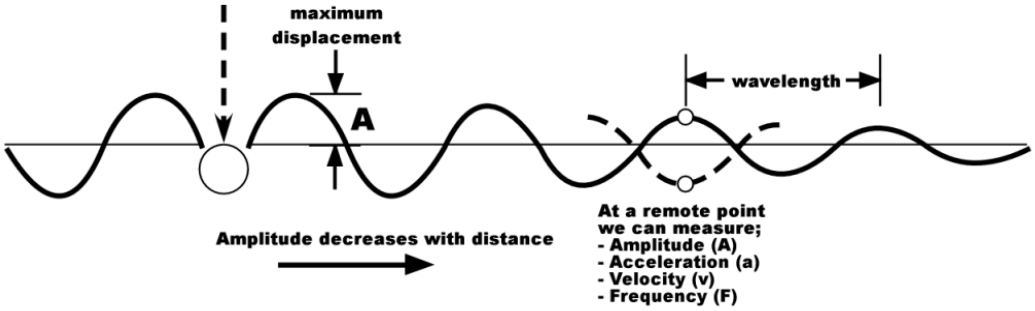

Figure 2.11 Blast wave terminologies [25]

Similar to the pond example, the ground vibration waves will disperse and diminish evenly in all directions in homogeneous rock conditions. Rock is an unreliable medium for vibration propagation, and blasts rarely contain just one charge. The many waves that make up the blast vibration originate from several holes, and the physical and structural characteristics of the earth they pass through govern how far they spread.

2.9 Ground Vibration Characteristics

2.9.1 Ground Vibration Principal

The transient movement or a time-varying displacement, velocity, or acceleration of a specific point (particle) in the ground due to rock blasting, piling, traffic, excavation, vibrating compaction, and other activities is commonly described as ground vibration or seismic energy [26]. Ground vibrations transmitted through the

ground may harm nearby structures when they reach a particular magnitude. A portion of the energy released after a blast travels through the shaft as seismic waves with various frequencies. Distance reduces the energy of these seismic waves, and the highest frequency waves are reduced the quickest [26]. This indicates that the blast's prominent frequencies are higher at close range and lower at a far range.

A typical particle velocity time history is displayed in Figure 2.12. When a vibration wave propagates, it has plus and negative peak amplitudes. A and B in Figure 2.12 denote the negative peak amplitude and plus peak amplitude, respectively. Peak amplitude, primary period (1/principal frequency), and vibration length are the three most crucial variables determining the time history. These variables are all influenced by the blast pattern and transmission medium.

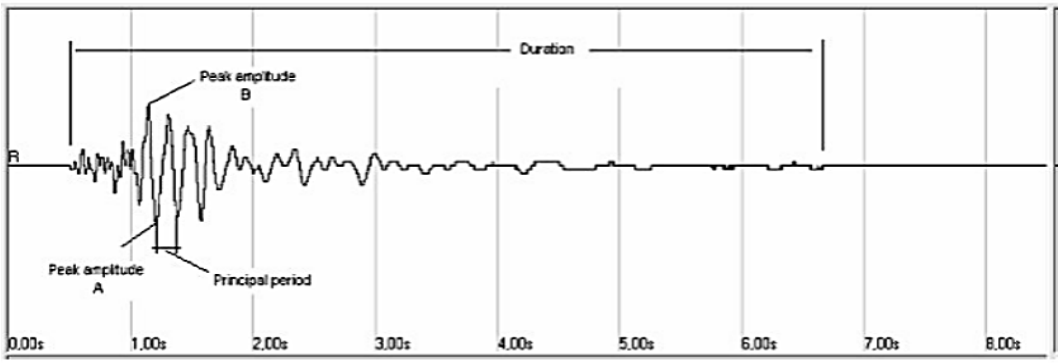

Figure 2.12 Typical blast vibration time history [26]

2.9.2 Peak Particle Velocity (PPV)

There are different forms of elastic waves, and they can travel within the ground. However, some of these waves are interconnected with ground vibration. These waves are; Surface waves, longitudinal and transverse, and they can travel to the depth of ground vertically or horizontally. Generally, the frequency range of the ground vibration varies from 1 to 200 Hz [27]. Lower-frequency waves (< 1 Hz) are known as microseisms, and they are commonly connected with natural phenomena such as ocean waves.

Ground vibration can be calculated in terms of Peak Particle Velocity (PPV) with unit mm/s [26]. Particle movement on the surface cannot relate to the PPV, only the particles movement within the ground can relate to PPV. Although, the displacement value in millimeters (mm) relates to particle movement at the surface. According to the United States Bureau of Mines [28], PPV is the velocity that is most closely related to the commencement of damage, that's why it is always measured. Each trace contains a point when the velocity is at its highest (+ve or -ve), which is known as the Peak Particle Velocity (PPV), which is measured in millimeters per second (mm/s) (in/s) (cm/s). The maximum accepted safe PPV value in the USA, China, and other parts of the world is 2 in/sec (50 mm/s) in the frequency range of 40-100 Hz [28].

2.9.2.1 Peak Particle Velocity as Damage Criteria

In 1958, the state of Pennsylvania became the first to adopt the Langefors, Kihlström [29], and Westerberg particle velocity Criterion to evaluate the potential for damage caused by ground vibration. This criterion established a 2.0 in/sec threshold as an acceptable maximum for most residential buildings. Figure 2.13 shows the correlation between the peak particle velocity and the frequency at which damage occurs.

Damage Effect	Peak Particle Velocity					
	Sand, gravel, clay below water; c = 1,000-1,500 m/sec		Moraine, slate, or soft limestone; c = 2,000-3,000 m/sec		Granite, hard limestone, diabase; c = 4,500-6,000 m/sec	
	mm/sec	in/sec	mm/sec	in/sec	mm/sec	in/sec
No noticeable crack formation	18	0.71	35	1.4	70	2.8
Fine cracks & falling plaster	30	1.2	55	2.2	100	3.9
Crack formation	40	1.6	80	3.2	150	5.9
Severe crack	60	2.4	115	4.5	225	8.9

Figure 2.13 Damage effects and PPV

The USBM's [30, 31] criterion safe blasting vibration for residential structures was designed in response to concerns about the effects of blasting on people's health and safety. For blasting operations, the maximum allowable ground vibration is between 0.5 and 2.0 in/sec for peak particle velocities, with a strong discontinuity at 40 Hz. High-frequency explosions (>40 Hz), such as those typically produced by nearby construction and excavation blasts, were found to have significantly larger damage potentials than low-frequency blasts (40 Hz) based on the criterion.

In 1993, German DIN established criteria for the impacts of vibration on structures, taking into account peak particle velocity, frequency, and type of structure [31]. Figures 2.14 and 2.15 show this criterion.

Line	Type of Structure	Vibration Velocity (mm/sec)		
		Foundation Frequency		
		Less than 10 Hz	10 to 50 Hz	50 to 100* Hz
1	Buildings used for commercial purposes, industrial buildings and buildings of similar design	20	20 to 40	40 to 50
2	Dwelling and buildings of similar design	5	5 to 15	15 to 20
3	Structures that, because of their sensitivity to vibration, do not correspond to those listed in lines 1 and 2 and are of great intrinsic value	3	8 to 10	8 to 10
* For frequency above 100 Hz, at least the values specified in this column shall be applied				

Figure 2.14 German DIN Standard Criterion for Vibration [31]

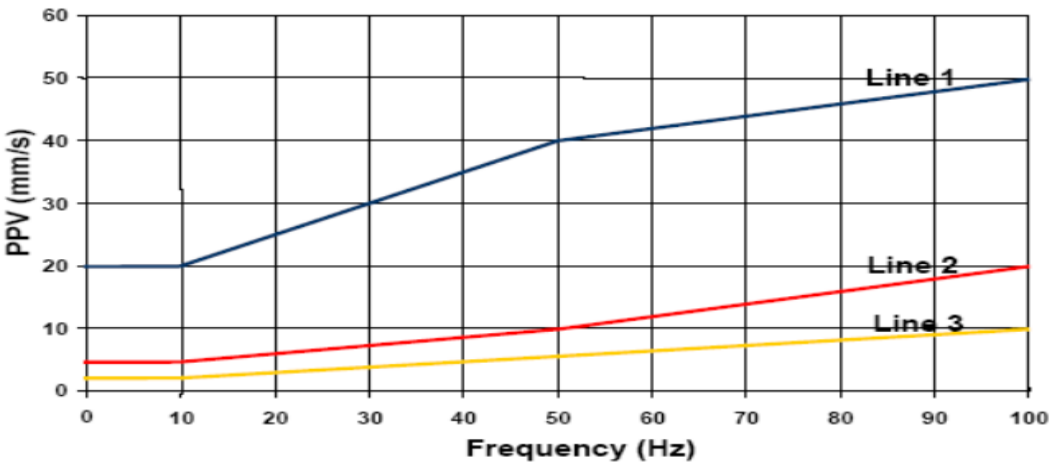

Figure 2.15 Ground vibration velocity representation curve versus frequency [31]

2.10 Prediction of Ground Vibration

Numerous researchers have explored the issue of predicting ground vibrations and developed numerous formulas. Although not an exhaustive list, the following equations illustrate the various methods used:

2.10.1 Langefors Formula (Langefors and Kihlstrom, 1973)

The following equation (4) was derived from Langefors and Kihlstrom's early studies on blasting in hard Swedish granite [29]. The rock transmission factor accepts various rock kinds and confinement settings, such as K = 400 for hard granite.

$$V = k\left(\sqrt{\frac{D}{\sqrt{Q}}}\right)^{-e} \qquad \text{Equation (2.4)}$$

Where:

K = Rock transmission factor

V = Peak particle velocity (mm/s)

Q = Maximum charge per delay (kg)

D = Blasting site to monitoring station distance (m)

e = Blasting site exponent

2.10.2 Scaled Distance Formula

Square root scale distance:

$$V = \frac{D}{\sqrt{Q}} \qquad \text{Equation (2.5)}$$

Cube root scaled distance:

$$V = \frac{D}{\sqrt[3]{Q}} \qquad \text{Equation (2.6)}$$

Where:

Q = Instantaneous charge mass (kg)

V = Peak particle velocity (mm/s)

D = Blasting site to monitoring station distance (m)

Both of these formulas were derived from studies conducted in the United States, with the majority of the focus on coal overburden blasting. There is considerable debate as to which is more suited, despite both having had positive outcomes.

Since the charge is distributed in a long cylindrical blasthole, the diameter of the hole is proportional to the square root of the charge weight. This scaled distance method is the most often utilized and is based on this fact. One may counter that the charge mass approaches a spherical form when the hole length shrinks with respect to the diameter, in which case the diameter would be proportional to the cube root of the charge weight.

The energy decay may vary depending on what waveform the energy is wasted in. It was already mentioned that surface waves prevail at particular locations (like coal mines). At other locations, body waves are the major mode of energy loss. The charge mass may have a more complex function than either the square or cube root, as well as the general equation, at different sites with various explosive designs and types of vibration waves created [32].

$$V = k\left(\sqrt{\frac{D}{Q^n}}\right)^{-1.6} \qquad \text{Equation (2.7)}$$

The square root scaled distance formula's practical use has been to gather information from several explosions, perform statistical analysis to identify the site constant "k" and site exponent "e," and then create a predicted formula like the frequently quoted:

$$V = 1140\left(\sqrt{\frac{D}{\sqrt{Q}}}\right)^{-1.6} \qquad \text{Equation (2.8)}$$

To make the calculating process simpler, this can then be prepared in the form of a table or chart, as seen in Figures 2.16 and 2.17.

PEAK PARTICLE VELOCITY (mm/s) AS FUNCTION OF CHARGE WT AND DISTANCE

Charge Wt per Delay / kg	Distance From Charge / m										
	5	10	20	50	100	200	500	1000	2000	5000	10000
0.25	28.6	9.45	3.12	0.72	0.24	0.08	0.02	0.01	0.00	0.00	0.00
0.50	49.9	16.4	5.43	1.25	0.41	0.14	0.03	0.01	0.00	0.00	0.00
0.75	69.0	22.7	7.50	1.73	0.57	0.19	0.04	0.01	0.00	0.00	0.00
1.00	86.8	28.6	9.45	2.18	0.72	0.24	0.05	0.02	0.01	0.00	0.00
1.50	120	39.6	13.1	3.02	0.99	0.33	0.08	0.02	0.01	0.00	0.00
2.50	181	59.6	19.7	4.54	1.50	0.49	0.11	0.04	0.01	0.00	0.00
5.00	315	104	34.2	7.90	2.61	0.86	0.20	0.07	0.02	0.00	0.00
7.50	435	144	47.3	10.9	3.61	1.19	0.27	0.09	0.03	0.01	0.00
10.00	548	181	59.6	13.8	4.54	1.50	0.35	0.11	0.04	0.01	0.00
15.00	758	250	82.4	19.0	6.28	2.07	0.48	0.16	0.05	0.01	0.00
25.00	1140	376	124	28.6	9.45	3.12	0.72	0.24	0.08	0.02	0.01
50.00	1985	655	216	49.9	16.4	5.43	1.25	0.41	0.14	0.03	0.01
75.00	2745	906	299	69.0	22.7	7.50	1.73	0.57	0.19	0.04	0.01
100.00	3456	1140	376	86.8	28.6	9.45	2.18	0.72	0.24	0.05	0.02
150.00	4780	1577	520	120	39.6	13.1	3.02	0.99	0.33	0.08	0.02
250.00	7193	2373	783	181	59.6	19.7	4.54	1.50	0.49	0.11	0.04
500.00	*****	4131	1363	315	104	34.2	7.90	2.61	0.86	0.20	0.07
750.00	*****	5714	1885	435	144	47.3	10.9	3.61	1.19	0.27	0.09
1000.00	*****	7193	2373	548	181	59.6	13.8	4.54	1.50	0.35	0.11
1500.00	*****	9949	3282	758	250	82.4	19.0	6.28	2.07	0.48	0.16
2500.00	*****	*****	4939	1140	376	124	28.6	9.45	3.12	0.72	0.24
5000.00	*****	*****	8599	1985	655	216	49.9	16.4	5.43	1.25	0.41

site law exponent = -1.60 site law constant = 1140

Figure 2.16 Square root scaled distance predictive model

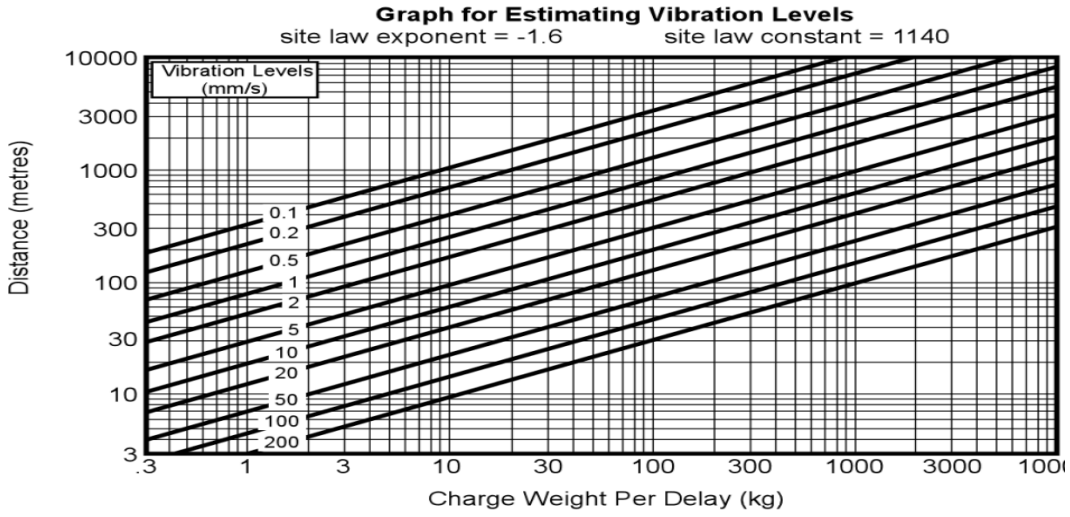

Figure 2.17 Square root scaled distance predictive chart

Then, the site constant can be altered to accommodate site confinement constraints. It may be reflected in formulas, like those found in AS2187.2, 1993, Table 2.1 [33].

Table 2.1 Firing to a free face hard or highly structured rock

Site Condition	K
Quarry	500
Average free face conditions	1140
Heavily confined conditions	5000

$$SD = \frac{D}{\sqrt{Q}}$$ Equation (2.9)

Where, SD is scaled distance, D is the blast-monitoring distance, and Q is the maximum charge per hole.

For instance, a scaled distance of 50 will provide protection from vibrations that exceed 51 mm/s. Vibrations larger than 25 mm/s will be protected by a scaled distance of 60.

With considerations for increasing confinement, this can also be rendered in chart form, as seen in Figure 2.18. Recognizing that ground vibration radially from an explosion varies significantly due to different ground conditions and other factors is important.

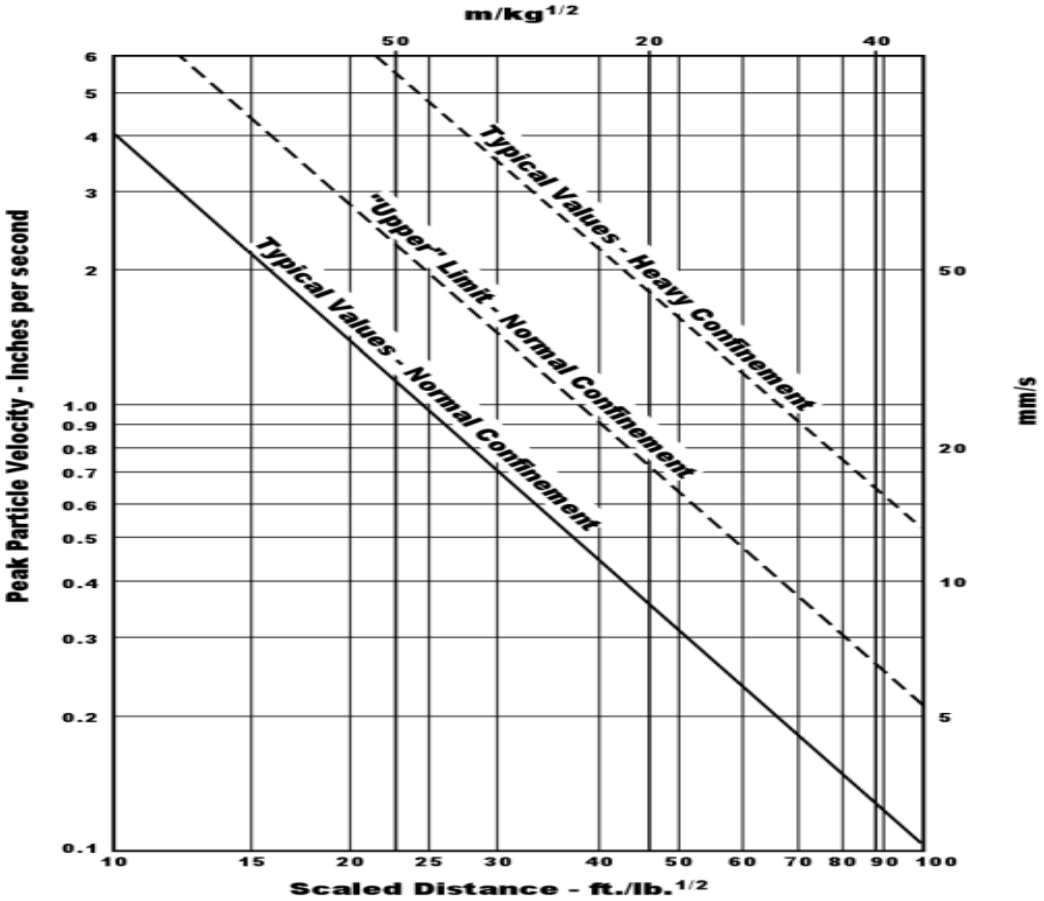

Figure 2.18 Increasing degrees of confinement and scaled distance chart [33]

According to Terrock Consulting Engineers' thorough examination of several blasts from numerous various sites and rock types, the site exponent of 1.5–1.8 is suitable for basalt flows with horizontal clay bottoms and sub horizontal coal mine overburden [33].

The site exponent varies with different types of rock, which significantly changes the site constant in the scaled-distance predictive model. For various rock types, typical site exponent values are listed in Figure 2.19.

Rock Type	Site exponent
Rhyodacite/Rhyolite	2.2 – 2.5
Granite	2.1 – 2.4
Limestone	2.1
Ordovican sediments	2.8
Coal mine overburden	1.5 – 1.8
Basalt (clay floor)	1.5 – 1.6
Basalt (massive)	1.9 – 3.0

Figure 2.19 Different rock type and exponent

High site exponents are significant because they lead to faster ground vibration decay and lower vibration levels at a distance. Figure 2.20, which displays the distance/PPV envelopes for several sites with various charge masses, emphasizes this.

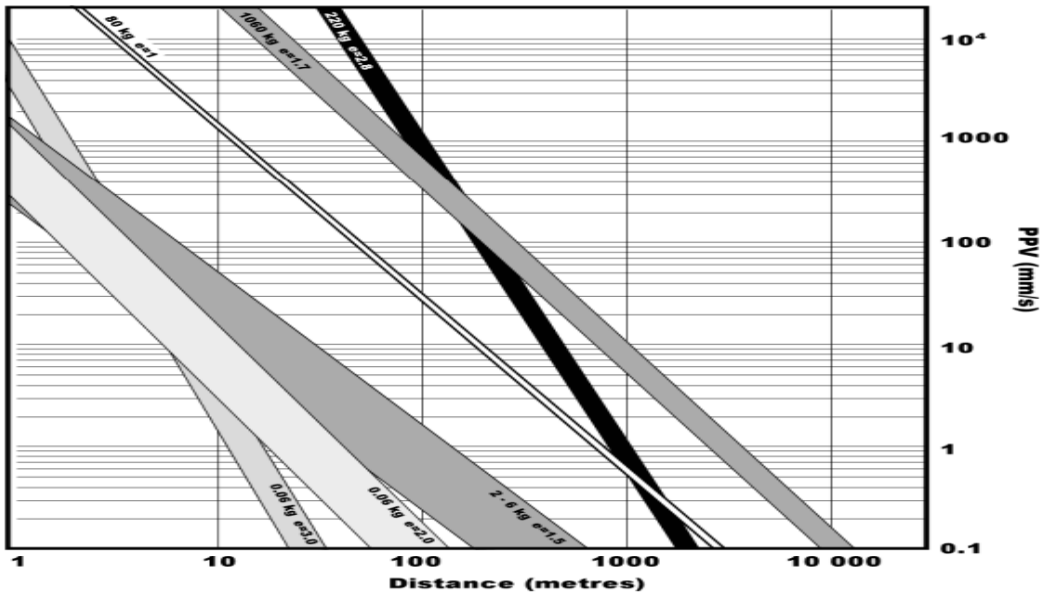

Figure 2.20 PPV and distance relationship for a number of sites [34]

2.11 Monitoring and Measuring Equipment

Using the rock in the pond as an example, a float on the water's surface would move up and down in the same spot as the waves passed by (as illustrated in Figure 2.5).

The float's motion can be measured. The impact of the wave on the float can be quantified by measuring its displacement (A), velocity (v), acceleration (a), and frequency (f). The three inter-related measurable parameters are as follow [35, 36]:

$$v = 2\pi fA \qquad \text{Equation (2.10)}$$

$$a = 2\pi f v \qquad \text{Equation (2.11)}$$

$$a = 4\pi^2 f^2 A \qquad \text{Equation (2.12)}$$

Correspondingly, it is possible to determine the displacement, particle velocity, particle acceleration, and frequency of ground vibration from a distance. Peak particle velocity correlates with damage more closely than peak displacement or peak

acceleration, as per experience. In order to assess ground vibration, devices that detect peak particle velocity are employed [36]. Blasting seismograph is the name given to these devices in most cases. Circuitry and a microphone are frequently found in blasting seismographs, allowing the analysis of air vibration signals.

The movement of the ground particles in three dimensions is complicated and elliptical due to the passage of blasting vibrations. The three mutually perpendicular components of the motion, namely the longitudinal (radial) (x), transverse (y), and vertical (z) components, must be measured in order to characterize the motion completely. The vector sum of the three components at a given instant in time represents the particle velocity at that place [35].

$$\textbf{Particle Velocity (PPV)} = \sqrt{V_x{}^2 + V_y{}^2 + V_z{}^2} \qquad \text{Equation (2.13)}$$

The peak particle velocity (PPV) is sum of the highest peak vector values. PPV is not the speed of the waves through the ground but rather the velocity of motion of a particle on or in the ground caused by the movement of the blast vibration waves.

A transducer, commonly a geophone, and an accelerometer can also be used, is linked to a CPU in a blasting seismograph to collect, process, and frequently store the data. The results are often printed on paper using a printer. The triaxial geophone comprises three transducers, each of which is composed of a moving mass system that is spring-loaded and encased in a moving coil. These transducers are mutually perpendicular to one another. The system moves in a magnetic field created by a permanent magnet. An electric current signal with a magnitude proportional to the coil's velocity is induced when the ground vibration moves the coil within the magnetic field. The signals are sent from the source to the processor via the cable.

Using transducers with a frequency response that covers the measurement range while taking blast vibration readings is crucial. Figures 2.21 and 2.22 display the frequency response curves for two geophone brands that adhere to the general specifications of AS2187-1993.

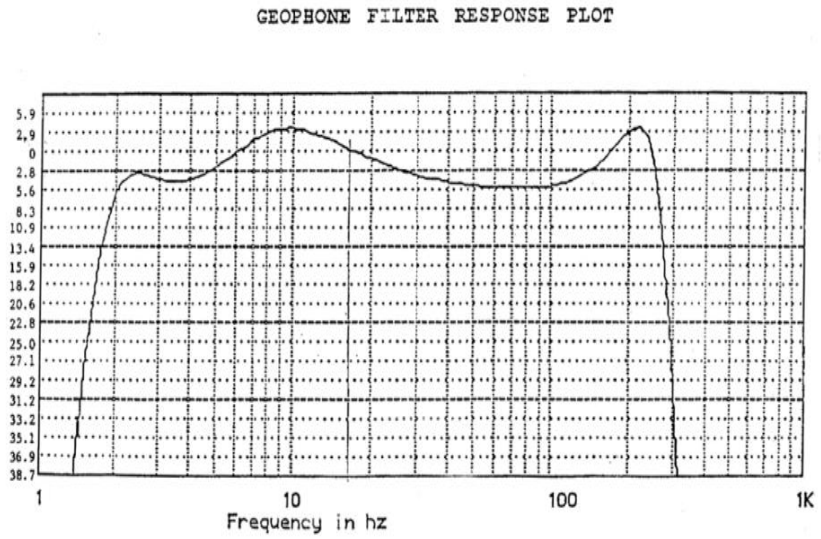

Figure 2.21 Frequency response-1 curves of geophone [35]

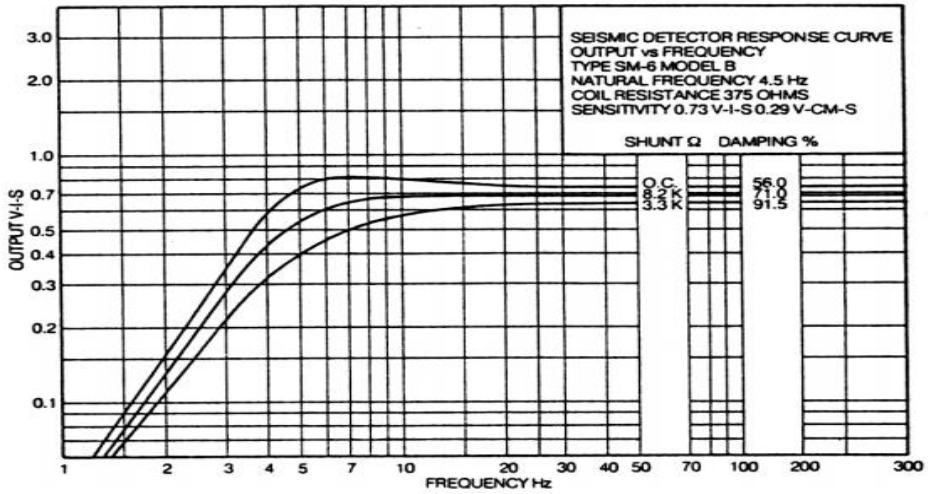

Figure 2.22 Frequency response-2 curves of geophone [35]

Major adjustments are needed for frequencies under 10 Hz. It is important to use caution when interchanging transducers because of the wide range of possible outputs.

Having the seismograph activated by the blast and the signal saved is usual practice due to limited data storage capacities and exposure to vibrations other than from blasting. Most seismographs allow customizing the recording's start and end times, as well as the trigger mode and level.

It is crucial to adapt the trigger method and trigger sensitivity to the specific needs of a project. The threshold should be low enough to detect the blast but not disturbed by everyday noises like passing cars or the hum of a blender [37].

Except across extremely long distances, ground vibration is the usual mechanism of the trigger. Because wind gusts typically produce vibrations greater than the blast's, air vibration can only be employed reliably on calm days. Furthermore, at 1 km, the ground vibration comes roughly 3 seconds before the air vibration. Therefore extra pre-trigger time is required to record the ground vibration signal if air vibration is employed as a trigger.

Different instruments with different working principles have been developed with time for the measurement of ground vibration. Some of the early instruments developed were mechanical and their working principle was that they contained heavy objects suspended from spring, as inert mass. However, after a blast or any kind of vibration; the instrument moved but the weight did not. After recording movements of the spring on the paper, the ground vibration was then possible to evaluate [38]. Nowadays, these instruments are replaced by electronic instruments; which are very easy to use and the results are very accurate.

An electrodynamics transducer called a geophone is used to convert mechanical sensed vibration into an electric signal in the electronic instruments for measuring ground vibration. The electric signal given by the transducer is directly proportional to the velocity of the vibration. This is how PPV can be recorded.

Three main types of ground vibration sensors are available in market [38];

- Displacement based sensor
- Velocity based sensor
- Acceleration based sensor

Some of the famous and latest monitoring instruments are the SuperGraph Minimate pro4, Mini SuperGraph and Blastmate. These are digital vibration and overpressure monitoring seismographs instruments; these instruments will be used in this study Figure 2.23, Figure 2.24, Figure 2.25 and Figure 2.26.

Figure 2.23 SuperGraph

Figure 2.24 Minimate Pro4

Figure 2.25 MiniSuper graph

Figure 2.26 Blastmate

2.12 Fragmentation

Blasting is the first step in the rock comminution process and it has a major impact on subsequent operations such as loading, hauling, crushing and grinding [39]. The uniformity of the muck pile benefits its dig ability which makes loading and hauling of the material easier and less time consuming [40]. The amount of oversize boulders produced by a blast defines how much resources will be used to further decrease their size in order for them to be effectively handled by the mining equipment.

Two processes that are significantly influenced by blasting are crushing and grinding. The parameter that has to be investigated here is the size distribution of the fragments from the blast. Increased coarse material in a muck pile will require more energy during the crushing and grinding stages [41]. It will also reduce the primary crusher's output because more material needs to be downsized.

The effect of blasting in the grinding stages of the comminution process has been investigated by Nielsen and Kristiansen, (1996) and Workman and Eloranta, (2003) [42, 43]. It is suggested that apart from fragmenting the rock, blasting also preconditions the fragmented material through the development of micro-fractures within the individual fragments. These micro-fractures develop through and around mineral grains and they are small enough to survive the initial crushing stages.

There is evidence that the micro-fractures weaken the individual fragments, which reduces the overall energy required in the grinding stages to achieve the desired fragment size (Bond’s work index) [44].

2.13 Influence of Geological Structures on Fragmentation

The fragmentation results of an explosion are highly sensitive to the characteristics of the rock mass being blasted. Fragmentation can be affected by various rock parameters, including compressive strength, porosity, density, Young's modulus, Poisson's Ratio, and the presence of fracturing and jointing in the rock [45]. Fragmentation crack network formation can be dampened and the energy distribution disrupted by the presence of rock structures, fracture planes, and voids. Both of these

can result in subpar blast fragmentation efficiency. Unless rock structures are mapped and identified, fragmentation will be poor if blast hole pattern dimensions are larger than the spacing between structures [46].

In 2013, Abu Bakar et al. analyzed how geological discontinuities affect fragmentation [43]. Fissures are present in most rock masses; they lower the rock's induced stress and stop the spread of radial cracks caused by blasting when the stress concentration drops too low. Blasting can generate fractures; however, the fracture pattern can be altered by the stress-time history of the material and by changes in the principal stresses. Junction infilling can impact wave transmission across the joint, depending on how well the infill material matches the impedance of the rock mass. Energy loss in joints increases with joint size. The wave transmission is enhanced for small joints with well-matched infill material compared to bigger joints or those with mismatched infill [43].

However, determining the strength of a rock mass, which affects fragmentation, can be challenging when the rock is not homogeneous. Bedding planes are a key factor in determining the overall stability of a rock mass. As a result of their presence, the stability of a rock mass is reduced, making it more susceptible to breaking up. The ability of bedding planes to regulate maximum fragmentation size also improves with the number of bedding planes in a rock mass. Because of the bedding at the base of the bench, it is much simpler to go around and more effective to break up the bench into smaller pieces [45]. Weathering of the rock mass can also affect fragmentation by forming rock zones with different strengths that differ from the rock below or around a contact zone.

2.14 Impact of Fragmentation on Blast Performance

The effectiveness of a blast can be measured in various ways. Traditionally, blast effectiveness was evaluated based on outcome results, but since these do not cover all of the areas that blast performance affects, evaluation of downstream results are now required [39]. Optimizing crusher and grinder throughput, reducing wear on

equipment, increasing dig rate and payload, decreasing energy consumption, and controlling fines production are all outcomes of effective rock fragmentation that contribute to lowering downstream costs. High-speed video, vibration monitoring, and photographic fragmentation analysis provide quantitative measures of blast effectiveness that operations can use to customize blasts to meet downstream goals.

2.15 Prediction Models for Fragmentation

Through the years, a number of different models developed to describe the size distribution of the fragments after blasting. Most of these models offer equations to calculate the average fragment size (X_{50}) as well as the entire fragment size distribution curve. The input for such models includes explosive material properties such as the weight strength, geometrical design features from the blast such as burden, spacing and bench height as well as in situ rock properties like discontinuity spacing, orientation etc.

While explosive properties and blast geometrical features are relatively easy to obtain and can be quite accurate, the same cannot be said for rock properties. The consideration of the rock mass as homogenous as well as the existence and properties of discontinuities throughout the rock mass make the rock properties difficult to establish and, in most cases, assumptions have to be made which will reduce the model's ability to accurately reproduce the fragment size distribution curve [47]. However, the trends indicated by the model's predictions are assumed to be correct and are used to provide blast design guidelines.

Although the blast fragmentation models predict the mesh size of the individual fragments, they give no prediction for their shape or the degree of preconditioning due to the generation of micro-cracks from blasting. Moreover, numerous small gaps can influence rock strength, while large voids can affect fragmentation because they enable gas to escape, decreasing gas pressure.

2.16 Rock Fragmentation Analysis

There are a variety of methods that can be used to assess the distribution of rock fragmentation. There is a wide spectrum of complexity among these techniques,

from the easy and qualitative to the tough and quantitative. Shot-to-shot qualitative fragmentation evaluation is possible via blaster observation and loader operator feedback on fragment size and diggability. This approach is not data-driven and is very susceptible to prejudice and inaccuracy due to its reliance on human judgment [40]. Although sieving shot rock provides an extremely precise quantitative method for evaluating fragmentation size, it is impractical, expensive, and time-consuming for use in actual mining operations. On the other hand, digital image analysis offers a practical solution for collecting the fragmentation results of bench blasts, as it bridges the gap between the two extreme approaches by providing a quantitative measure of fragmentation sizing with no interference to the mining process [41]. Digital image analysis of blasted rock can be conducted using images of the muck pile taken with hand-held/portable cameras, belt-mounted systems, or loader-mounted systems.

Various software packages and image-capturing methods can facilitate digital image analysis for fragmentation sizing. Wip Frag, imageJ, Split Desktop, Gold Size, Frag scan, Power Sieve, and BLASTFRAG are just a few examples. Most image analysis tools function comparably, and all of them need a scale object to be included in the picture. Wip Frag is a program that can take a picture of a rock pile or other shattered rock and turn it into a mesh of individual pieces. In order to simulate a sieve and sort the pieces, the net is measured. The D10, mean, D50, and D90, as well as graphs of the fragmentation sizing, are provided. "pictures must be clear, evenly lighted, and must be gathered systematically in order to reduce modification and optimize outcomes," WipFrag (2015) [48] says. Editing the rock outline is usually required, even when high-quality photographs are used, in order to differentiate between fragments, identify fines, and exclude shadows or other areas from the study. Photos should be taken after the shot and as mucking progress to ensure nothing of interest is missed.

It is important to be aware of the limitations of digital image analysis before using it to optimize fragmentation however this does not affect the analysis' effectiveness. Among these is the laborious process of hand-editing rock outlines for precise fragment delineation. The analysis becomes more susceptible to human

mistakes, especially at the smallest particle sizes. This inaccuracy is reduced to a minimum in high-resolution photos or those containing larger-than-average particles. Other problems include mistakes in the calculations used to convert rock surface measurements into volumes, low-resolution imaging systems, shape effects that give fragments different mesh sizes in the imaging analysis than they would have in sieving, and density assumptions. Some of these issues, like the volume calculations, become inconsequential when using image analysis to make side-by-side comparisons, as any error introduced will apply to all of the images, and the variation in size distribution between photos will still be obvious. Despite the drawbacks, investigations have shown that the size distributions obtained by digital image analysis of muckpiles are comparable to those of sieved material. Material mistakes are less common when working with coarse rather than fine materials.

CHAPTER 3

METHODOLOGY

3.1 Flowchart of Study

This section explains the research's study area, materials, and methods adopted. Figure 3.1 shows the flow of research methodology.

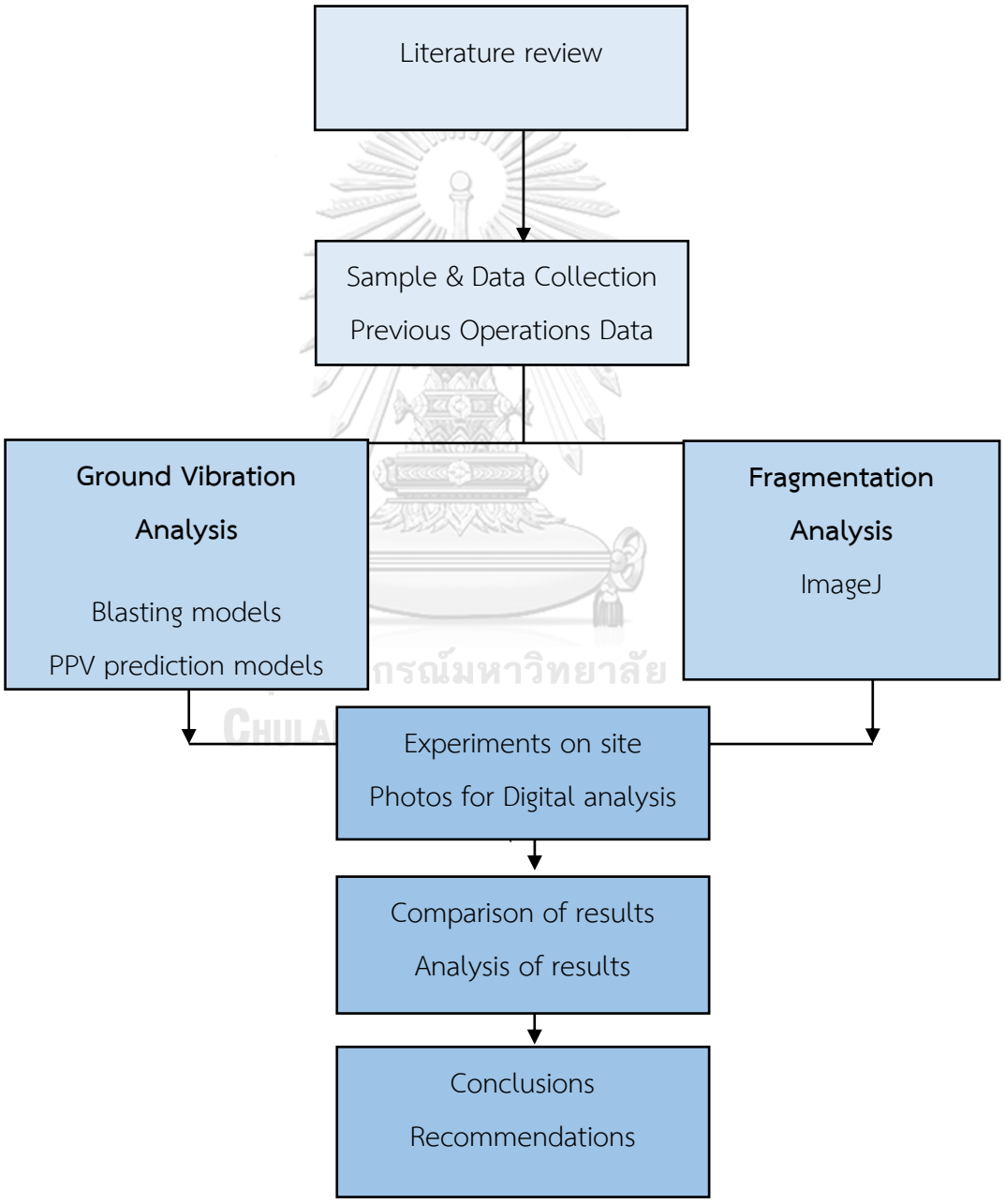

Figure 3.1 Research Methodology

3.2 Site Location

The Khao Mai Nuan pyrophyllite quarry is located at Cha-Om Village, Kaeng Khoi District, Saraburi Province, Thailand. According to the topographic map of the Royal Thai survey department, 95-02-59 Rai of area of the quarry is located on the sheet name Amphoe Banna, sheet no. 5237 IV, series no. L 7017(Map scale 1:50,000) falls on latitude 1594000 – 1595000 N and longitude 726000 – 727000 E. Figure 3.2 shows the road map and study area location, and Figure 3.3 shows the mineral resource of pyrophyllite.

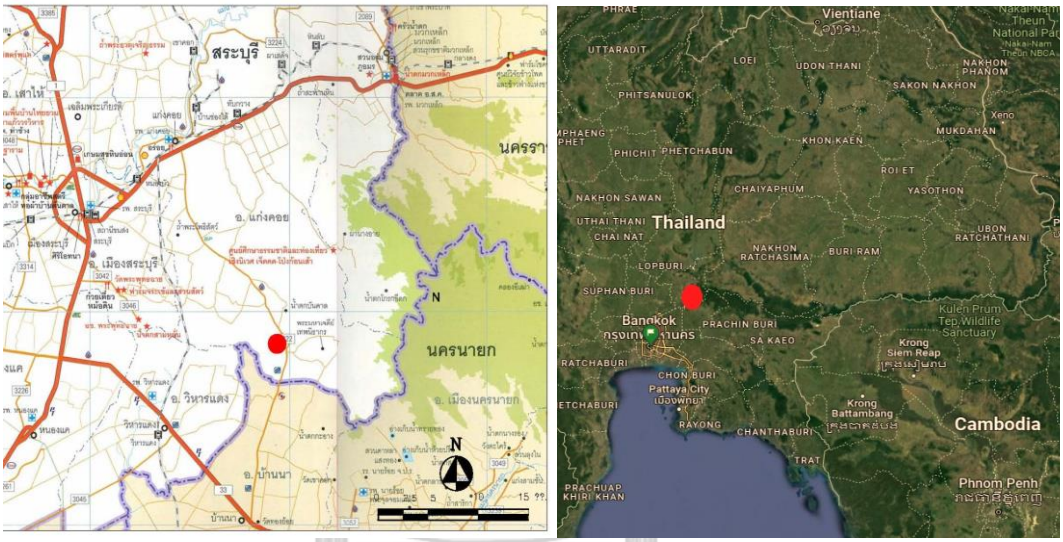

Figure 3.2 Roadmap and study area location

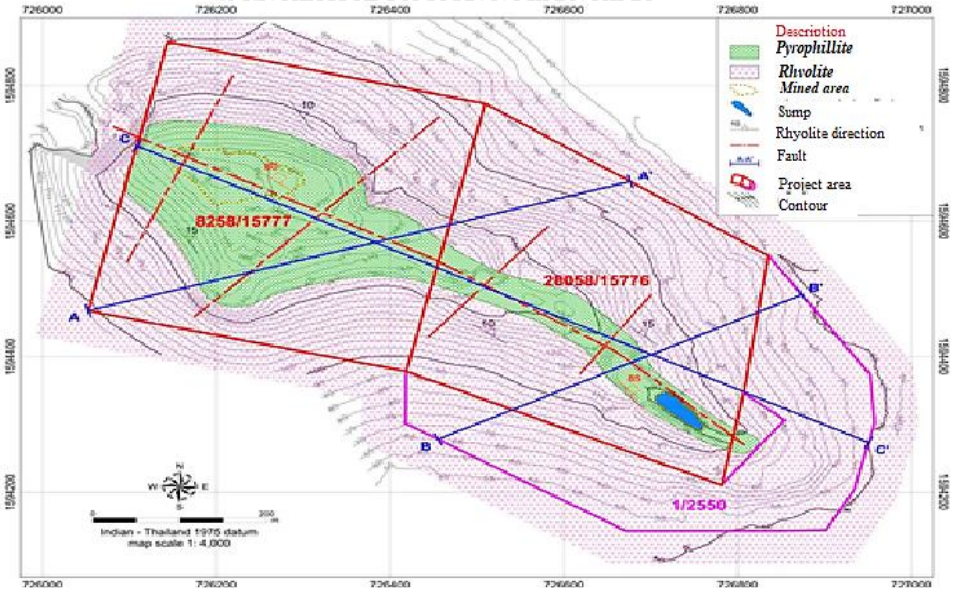

Figure 3.3 Map showing Pyrophyllite resource

3.3 Geology

Pyrophyllite is a mineral composed of hydrous aluminum silicate with the standard chemical formula $((Al_2SiO_4O_{10}(OH_2))$. The chemical composition of pyrophyllite in a pure state is 66.65% SiO_2, 28.35% Al_2O_3, and 5% H_2o [49]. It is a rare metamorphic mineral commonly associated with clay minerals, such as quartz, mica, topaz, kaolinite, and rutile.

The formation of pyrophyllite from its parent rock is a combined process of hydrothermal alteration, and low-medium grade metamorphism, which results in the loss of alkalis, iron, and gaining of alumina [50]. The presence of quartz in the zones of pyrophyllite shows the silica activity during the formation of pyrophyllite. In addition, the mineralogy and petrology of pyrophyllite quarry show leaching activities, e.g., weathering and alteration, which help leach silica without disturbing the alumina content. The percentage of alumina and silica contents in pyrophyllite indicates grade. A sample with a high percentage of Al_2O_3 is considered high grade and vice versa. The color of the pyrophyllite changes with different specific gravity.

3.4 Problem Identification

The literature review identified that improper blast design could cause excess ground vibration and unwanted fragmentation. With optimization of various blasting parameters can reduce the risk of ground vibration and the production of unwanted fragmentation. This topic of study has become very important in the 21st century as these blasting impacts directly affect the environment and disturb the nearby humans, public properties, and national resources. This study aims to ascertain blasting design based on the optimized controllable parameters, which will lead the blasting operations towards better fragmentation size and approved ground vibrations level at the Khao Mai Nuan pyrophyllite quarry, Saraburi, Thailand.

3.5 Collection of Samples and Testing

Grab samples from the study area were tested in the rock mechanics lab. Point load test, Uniaxial Compressive Strength (UCS) test, and Brazilian test were done to find the strength of the pyrophyllite rock samples.

3.5.1 Determination of Rock Strength

3.5.1.1 Point load Test

The point load test is designed to evaluate the strength of rock materials. Because it is an index test, it may rapidly and easily provide crucial information about rocks' mechanical characteristics without using additional tools [31].

It is possible to do point load testing on non-rectangular blocks that have a rectangular prism-like geometry. When the height of a block is held constant, and its top and bottom bases $(w_1 \text{ and } w_2)$ are parallel, we call the resulting shape a trapezoid (D). A formula of $W = (w_1 + w_2)/2$ is used to get the mean width, and the loading technique is similar to that of the Block Lump Test. The specimen's geometry and the loading forces applied during the point load test are illustrated in a schematic form in Figure 3.4.

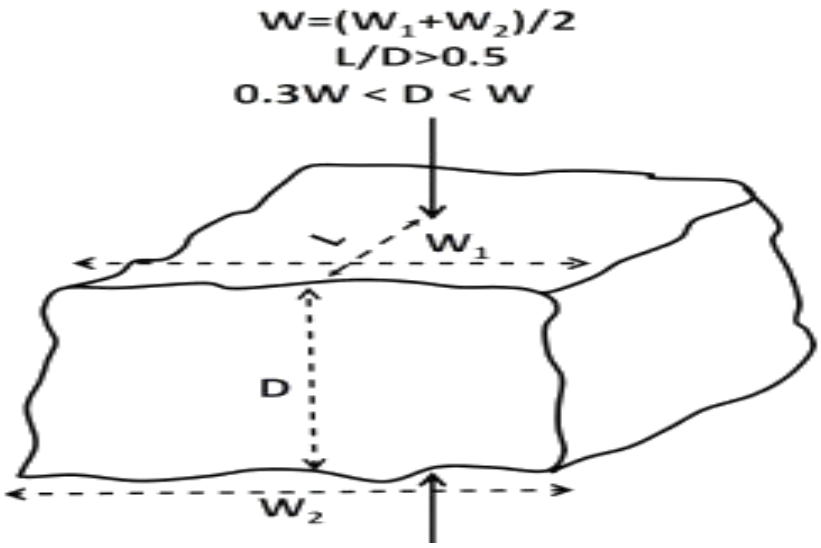

Figure 3.4 Lump sample test requirements

Samples were prepared mostly in rectangular shapes, with different diameters, lengths, and widths as shown in Figure 3.5. Sample after the breakage is shown in Figure 3.6. The standard method for the point load test, as described by Bienniawski, Z.T., 1975; ISRM, 1995; and ASTM, 1994), was followed.

Figure 3.5 Prepared samples before point load test

Figure 3.6 Sample after point load test

3.5.1.2 Uniaxial Compressive Strength (UCS)

Samples were prepared according to the instructions provided by ISRM, 1995 and ASTM, 1994 [27]. The hydraulic core cutting machine shown in Figure 3.7 was used for sample preparation, having an inner diameter of 5.4 cm and a height of 10.8 cm. Core samples are illustrated in Figure 3.8.

Figure 3.7 Core samples preparation

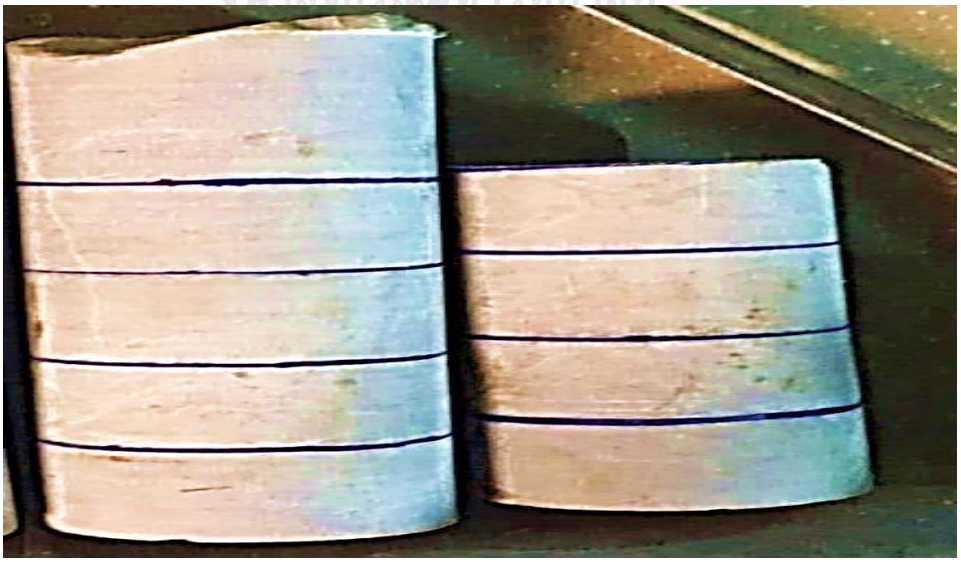

Figure 3.8 Prepared core samples for UCS

Samples were tested and the value of peak load (kN) and Peak stress (kPa) were recorded in order to find the Uniaxial Compressive Strength (UCS) or σ_C or U_c.

$$\sigma_C = \frac{F}{A} = \frac{\text{Peak load}}{\text{Cross sectional area}} \qquad \text{Equation (3.1)}$$

Where:

σ_C = Uniaxial Compressive Strength (MPa)

F = Peak load (N)

A = Cross sectional area (mm^2)

3.5.1.3 Brazilian Test

Samples were prepared by using a core drilling machine shown in Figure 3.7. The core samples are then cut into specific dimensions with the help of a core cutting machine, as illustrated in Figure 3.9. The height of the core samples is equal to 0.5 of the diameter of the core, according to ISRM, 1978. Our sample's height was 2.7 to 3 cm, as shown in Figure 3.10.

Figure 3.9 Core cutting illustration

Figure 3.10 Prepared samples for Brazilian test

Samples were tested with the help of a universal testing machine illustrated in Figure 3.11. Peak load (kN) and peak stress at failure (kPa) values were recorded to find the samples' tensile strength

$$\sigma_t = \frac{2L}{\pi Dh} \qquad \text{Equation (3.2)}$$

Where:

σ_t = Tensile Strength (MPa)

L = Force reading from the equipment (N)

D = Diameter of sample (mm)

h = Height of sample (mm)

Figure 3.11 Tensile strength testing machine

3.5.2 XRD and XRF Analysis

Proper sample preparation is essential to getting high quality XRD and XRF data. Initially, the samples were crushed into small pieces to feed into the disc mill machine. Figure 3.12 shows the prepared samples for the disc mill. After crushing, the samples were ground into 75 um with the help of a disc mill, as shown in Figure 3.13.

As the samples were not completely dry, we put them in the oven for 3 hours to dry them thoroughly. Five samples of 5 grams each were prepared and sent to the XRD and XRF Laboratory.

Figure 3.12 Crushed samples for XRD and XRF

Figure 3.13 Disc Mill

3.5.2.1 XRD Analysis

An X-ray diffraction (XRD) analysis of pyrophyllite was done to study the crystal structure and reveal the mineral composition. Knowledge of the compositions is vital for understanding pyrophyllite's quality/grade and adverse health impact.

X-ray diffraction (XRD) analyses were done using Chulalongkorn University research facilities. The D8 Advance Bruker machine (Figure 3.14) was used for XRD analysis using the direct filter paper method and DIFFRAC.EVA software for the analysis of XRD results.

Figure 3.14 D8 Advance Bruker machine

3.5.2.2 XRF Analysis

XRF analysis was done to determine the elemental composition of pyrophyllite, as XRF spectroscopy is an excellent technology for qualitative and quantitative chemical composition analysis. Moreover, it also helps to select the

excellent grade area of the quarry for future operation at the quarry. XRF analyses were also done using Chulalongkorn University research facilities.

3.6 Optimization of the Blasting Design Parameters

The Swedish method created by Langefors and Kilhstrom was used to determine the parameters (1978). The geometric layout of the blasting pattern in this case and the computation of the charges are based on the rock's Uniaxial Compressive Strength. Figure 3.15 displays the approximations for the geometric parameter values as a function of the compressive rock strength. The stemming length and sub-drilling were also estimated according to the blast hole diameter and compressive rock strength. Figure 3.16 provides the suggested lengths of bottom charges.

Design parameter	Uniaxial Compressive Strength (MPa)			
	Low	Medium	High	Very High
	<70	70 – 120	120 – 180	>180
Burden	39D	37D	35D	33D
Spacing	51D	47D	43D	38D
Stemming	35D	34D	32D	30D
Sub-drilling	19D	11D	12D	12D

Figure 3.15 Geometric parameters variation with UCS

Design parameter	Uniaxial Compressive Strength (MPa)			
	Low	Medium	High	Very High
	<70	70 – 120	120 – 180	>180
Bottom charge Length	30D	35D	40D	46D

Figure 3.16 Bottom charge length variation with UCS

3.7 Blast Designs

Four different modified blast designs were used throughout field investigations. Each design was based on different theories, empirical equations, and the strength parameters of the pyrophyllite rock mass.

3.7.1 UCS Based Design

The initial blast was conducted with a slightly revised plan based on the pyrophyllite rock's Uniaxial Compressive Strength. Major parameters like burden, spacing, stemming, sub-drilling, and bottom charge were calculated using Figure 3.15 and 3.16.

3.7.2 Dyno Nobel Pacific Pty Limited 2020

The explosive engineer's guide published in 2020 by Dyno Nobel was used during the second modified blast design [14]. Rules of thumb were employed to determine the different controllable parameters of the blast design. Figure 3.17 shows the empirical formulas and parameters calculations.

RULES OF THUMB			
Parameter	Calculation	Parameter	Calculation
Blasthole diameter (D)	15 x BH (mm)	Bench Height (BH)	D/25 (m)
Burden (B)	30 x D (m)	Spacing (SP)	1.15 x D (m)
Sub-drill (SD)	7.5 x D (m)	Charge length (C)	20 x D (m)
Stemming (S)	0.5 x B (m)	Hole length (L)	BH + SD (m)

Figure 3.17 Dyno Nobel Limited 2020 rules for blast design [14]

3.7.3 Stig O Olofson

The blast design proposed by Stig O Olofson in 1989 was used for the third modified blast at the pyrophyllite mine. This blasting model is based on empirical

formulas and equations. Table 3.1 shows the empirical formulas to find the optimized parameters of blast design.

Table 3.1 Design proposed by Oloffson, 1988 [19]

Parameter	Calculation
Burden ($\mathbf{B_{max}}$)	$1.36\sqrt{i_b}$ (m)
Sub-drilling (Sd)	0.3 × $\mathbf{B_{max}}$ (m)
Hole length (Hl)	1.05 (Bench height + Sd) (m)
Error in drilling (E)	D/1000 +.03× Hl (m)
Practical Burden (B)	($\mathbf{B_{max}}$) – E (m)
Spacing (SP)	1.25 × B (m)
Stemming (S)	Practical Burden (m)
Charge length (Cl)	Hl – S (m)

3.7.4 Hybrid Design

The combination of Uniaxial Compressive Strength (UCS), Dyno Nobel Pacific Pty Limited 2020, and Stig O Olofson (1989) models were used to design the fifth blast. In this modified hybrid design-4, blast design parameters were calculated according to the site geometric properties, as the geology of the mine changed with bench height and location. Figure 3.15 – 3.17 and Table 3.1 shows the empirical formulas and parameter calculation equations.

CHAPTER 4

STRENGTH PARAMETERS OF PYROPHYLLITE

4.1 Point load Test

From the experiments, it is found that sample 5 (L = 60 mm, D = 37) has a peak UCS value of 109 MPa, and sample 2 (L = 70, D = 40) has the lowest UCS value of 73 MPa. After excluded the highest and lowest values of UCS, the average UCS value was 94 MPa. Tables 4.1 shows dimensions of the samples, and Table 4.2 shows UCS calculation.

Table 4.1 Samples dimensions

Sample	W_1 (mm)	W_2 (mm)	$W = \frac{W_1 + W_2}{2}$ (mm)	L (mm)	D (mm)	A= WxD (mm^2)	$D_e = \sqrt{\frac{4A}{\pi}}$ (mm)	L = L/D (mm)
1	60	65	62.5	80	50	3125	63.0	1.6
2	60	70	65.0	70	40	2600	57.5	1.7
3	40	30	35.0	70	30	1050	60.0	2.3
4	50	56	53.0	75	45	2385	55.0	1.6
5	65	55	60.0	60	37	2220	53.0	1.6

Table 4.2 Uniaxial Compressive Strength (UCS) calculation

P (kN)	$I_s = P/D_e^2$ (kN)	I_s (MPa)	$F = (D_e/50)^{0.45}$ (Size correction)	I_{50} (MPa)	$UCS = \alpha . I_{50}$ (MPa)
30	0.007559	7.5	1.1	9.7	97
20	0.006049	6.0	1.0	7.3	73
22	0.006111	6.4	0.8	9.7	97
15	0.004959	4.9	1.0	8.9	89
18	0.006408	6.4	1.0	10.9	109

4.2 Uniaxial Compressive Strength (UCS)

From the experiment, it is found that the sample U3 had stress equals 11.42 Pa (the maximum Stress), and Uniaxial Compressive Strength (UCS) equals 118.5 MPa (the highest Uniaxial Compressive Strength).

Sample U5 had stress equals 4.0 Pa (the minimum Stress), and Uniaxial Compressive Strength equals 50 MPa (the lowest Uniaxial Compressive Strength. The average Uniaxial Compressive Strength equals 85 MPa. Experimental data are shown in Table 4.3. Pre and post samples visuals can be found in the Appendix A.

Table 4.3 UCS Experimental data of Pyrophyllite

Sample	Hight (cm)	Peak load (kN)	Stress (Pa)	Uniaxial Compressive Strenght (MPa)
U1	12.3	146	6.2	64
U2	11.8	215	9.0	94
U3	12.1	271	11.5	118
U4	11.9	199	8.4	87
U5	12.3	115	4.0	50
U6	11.7	225	9.5	98
Average	**12**	**195**	**8.1**	**85**

4.3 Brazilian test

From the experiments, sample B19 had stress equals 6.5 Pa (the maximum stress), and the tensile strength equals 40 MPa (the highest tensile strength). Samples photos before and after the test can be found in Appendix B.

The B28 had stress equals 1.94 Pa (the minimum stress), and tensile strength equals 11 MPa (the lowest) tensile strength).

Given that every failure is valid and the selected loading rate was appropriate as all samples fail within the desired frame, the tensile strength of the pyrophyllite is calculated as the average value between 30 tests. Therefore, the average tensile strength equals 22 MPa. Experimental data are shown in Table 4.4.

Table 4.4 Brazilian test results

Sample	Height (cm)	Peak load (kN)	Stress (Pa)	Tensile strength (MPa)
B1	3.2	23	3.3	19
B2	3.1	21	3.0	16
B3	2.8	31	4.3	26
B4	2.9	33	4.6	25
B5	3.2	20	2.8	16
B6	3.3	20	2.7	15
B7	3.5	26	3.7	19
B8	2.8	23	3.2	18
B9	2.9	41	5.7	33
B10	3.1	23	3.2	18
B11	2.9	18	2.5	15
B12	3.0	24	3.3	18
B13	2.9	28	3.8	22
B14	3.2	30	4.2	23
B15	2.9	19	2.7	15
B16	3.1	36	5.1	27
B17	2.8	33	5.0	25
B18	2.8	39	5.4	33
B19	2.7	46	6.5	40
B20	3.2	28	3.9	20
B21	3.1	37	5.2	28
B22	2.9	36	5.0	28
B23	3.3	27	3.8	21
B24	2.9	36	5.0	29
B25	2.9	18	2.6	15
B26	2.8	18	2.5	15
B27	2.7	20	2.8	17
B28	3.2	14	1.9	11
B29	3.1	25	3.6	19
Average	**3.0**	**27**	**3.8**	**22**

4.4 XRD and XRF Analysis

XRD analysis shows the existence of different crystallographic forms. Figure 4.1 represents the obtained results from the diffraction spectrum. Quartz, Dickite Pyrophyllite, Berlinite, Almandine, and Rutile can be identified. All these components are alkaline, having a crystalline form and stable compounds.

The chemical analysis of pyrophyllite samples allows measuring the quantitative results. Table 4.5 summarizes the chemical analysis of pyrophyllite. Chemically, it is verified that sample is composed mainly of SiO_2 and Al_2O_3. These two components correspond to nearly 98%.

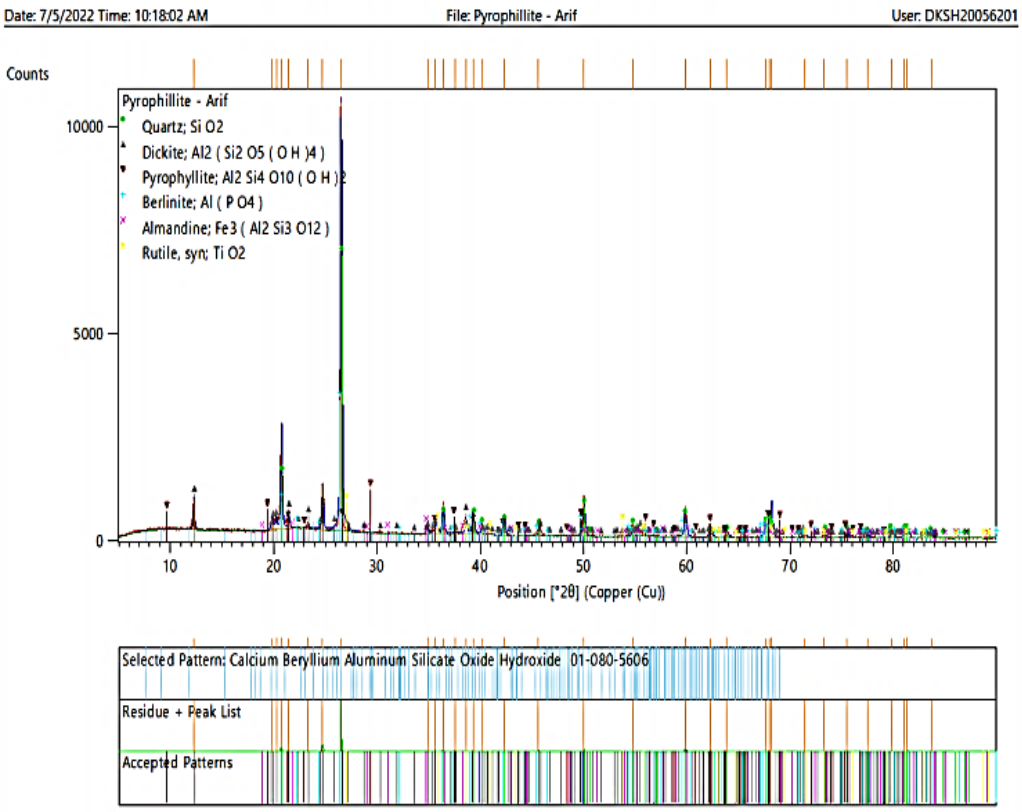

Figure 4.1 X-ray diffraction (XRD) analysis graph

Table 4.5 Chemical composition of Pyrophyllite

Compound	Concentration	Unit
SiO_2	78.2	%
Al_2O_3	20.6	%
P_2O_5	0.3	%
TiO_2	0.2	%
CaO	0.1	%
Fe_2O_3	0.1	%
Cr_2O_3	347.4	ppm
K_2o	228	ppm
V_2O_5	36.1	ppm
MnO	9.4	ppm

CHAPTER 5

EXPERIMENTS

5.1 Overview

All test blasts were conducted on different benches of a pyrophyllite quarry in Saraburi Province, Thailand. The test blasts conducted between June 2022 and September 2022 were full-size production blasts. All the test blasts were conducted during the field investigation timeframe using different design parameters, benches, and data collection procedures. Each test blast produced a muckpile weight of approximately 1500 tons.

5.2 Geometric Data of Current Blast Design

The current blast design parameters presented in Table 5.1 were obtained from the design plans and reports provided by SCG Ltd. The current conventional blast design employed the staggered drilling pattern and non-electric row-to-row initiation system.

Table 5.1 Blast design parameters of existing blast design

Parameter	Value
Hole Depth (m)	9
Hole Diameter (mm)	76
Burden (m)	2
Spacing (m)	3
Sub drilling (m)	1
Stemming (m)	2
Delay (mm/s)	25

5.3 Rock Parameters

Data obtained included the rock type, rock description, Uniaxial Compressive Strength, tensile strength, and rock density to optimize blast design and build the predictive models. The rock parameters of the pyrophyllite quarry are summarized in Table 5.2.

Table 5.2 Pyrophyllite Rock Mass parameters

Parameter	Value
Rock type	Pyrophyllite
UCS (MPa)	85.31
Tensile strength (MPa)	21.63
XRD	Rich in Pyrophyllite
XRF	98% of SiO_2 and Al_2O_3

5.4 Explosive Data

Thai Nitrate Co., LTD supplies bulk explosives for blasting operations at the Pyrophyllite quarry. The explosive used at this quarry is called Ammonium Nitrate, or ANFO, a highly unsensitized bulk explosive. A No. 8 blasting cap cannot detonate it without a sensitizer. A larger quantity of secondary explosive called pentolite is used as a booster to detonate ANFO at this mine. The parameters of ANFO are shown in Table 5.3.

Table 5.3 Parameters of ANFO

Parameter	ANFO
Specific gravity (g/cm^3)	0.82
Loading density (g/cm^3)	0.75 - 0.85
Detonation velocity (m/s)	3300
Water resistant	No
Energy (MJ/kg)	3.7

5.5 Instrumentation

Several ways were used to collect information about each blast conducted during the field investigation. However, the most important data was collected via high-resolution digital pictures taken after each blast for the fragmentation analysis. The photographs were taken carefully before and after each from different angles. These photographs were used to examine the bench and floor condition. Seismograph and other monitoring instruments were set up according to the blast location.

Coordinates of the blasting site and monitoring stations were determined using GPS (Global Positioning System). In addition, the absolute distance between the blasting site and the monitoring stations was also measured using the Global positioning system.

A ground vibration instrument called seismograph was used to monitor each blast and calculate the blast-induced vibration. Instantel Micromate was deployed to model digital ground vibration and airblast. Figure 5.1 shows instruments used in the research study.

Figure 5.1 Instantel Micromate

5.6 Test Blasts

The test blasts were conducted between June, 2022 and September, 2022. Each blast was set-up using the blast design, delay, explosive, bench, and instrumentation as stated earlier. The various blasting designs with optimized parameters according to the controllable and un-controllable factors were tested and the benches in which they were shot are summarized in Table 5.4.

Table 5.4 Summary of the blasts conducted at the Pyrophyllite quarry

Test Blast	Date	Design	Bench
1	24-06-2022	Conventional	3
2	24-06-2022	Modified-1	2
3	08-08-2022	Modified-2	1
4	09-08-2022	Modified-3	1
5	24-09-2022	Modified-4	3

5.6.1 Test Blast-1

On June 24, 2022, the first test blast was conducted. The blast occurred on the 3rd Bench at 2:00 PM. Figure 5.2 shows that the blast had 12 holes angled 5° toward the face and was designed to be drilled to a depth of 9 meters. The planned depth of the drill included a sub-drill of 1 meter, and the bench height was 8 meters. The planned burden was 2.5 meters, and the distance between blast holes was 3 meters. Most of the overburden occurred at the toe. Table 5.5 gives information about the bench face, blast design and profile. Figure 5.3 shows the location of test blast-1 on Google earth.

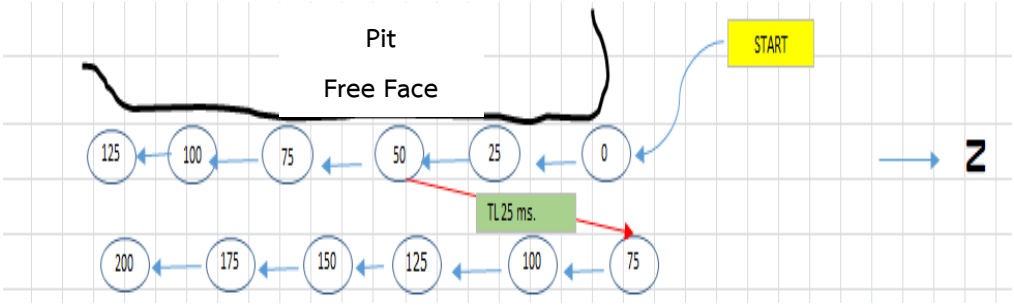

Figure 5.2 Drilling and initiation Pattern

Table 5.5 Current geometric blast design data

Current Blast Design			
Parameter	**Value**	**Parameter**	**Value**
Rock Type	Pyrophyllite	Borehole diameter (mm)	76
UCS (MPa)	85 (Medium)	Drilling Pattern	Rectangular
Density ($\mathbf{g/cm^3}$)	2.8	Initiation sequence	Staggered
Maximum Burden (m)	3	Minimum Burden (m)	2
Average Burden (m)	2.5	Charge length (m)	7
Spacing (m)	3	Charge per hole (ANFO) (kg)	22
Bench Height (m)	8	Total weight of charge (ANFO) (kg)	264
Sub drilling (m)	1	Booster per hole (Pentolite) (kg)	0.5
Number of Holes	12	Total weight of charge (ANFO+Pentolite) (kg)	270
Total weight of Booster (Pentolite) (Kg)	6	Yield in volume ($\mathbf{m^3}$)	720
Yield in Ton	2016	Powder Factor ($\mathbf{kg/m^3}$)	0.37

Figure 5.3 Location of the test blast-1

5.6.2 Test Blast-2

On June 24, 2022, the second test blast was done. The blast happened on the 3rd Bench at 2:30 p.m. Figure 5.4 shows that the blast had 10 holes angled 5° toward the face and was designed to be drilled to a depth of 10 meters. The planned depth of the drill included a sub-drill of 1 meter, and the bench height was 9 meters. The planned burden was 2 meters, and the distance between holes was 2.5 meters. The front row's burden was between 1.7 and 2.3 meters. Table 5.5 shows information about the blast design and the bench face profile. Figure 5.5 shows the location of test blast-2 on Google earth.

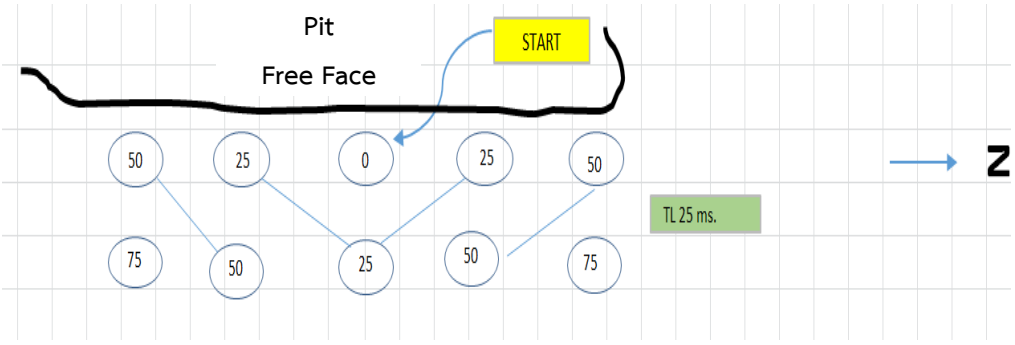

Figure 5.4 Drilling and initiation Pattern

Table 5.6 UCS based Blast Parameters

Modified Design-1			
Parameter	**Value**	**Parameter**	**Value**
Rock Type	Pyrophyllite	Hole Depth (m)	10
UCS (MPa)	85 (Medium)	Stemming (m)	2
Density of Pyrophyllite ($\mathbf{g/cm^3}$)	2.8	Number of Holes	10
Borehole diameter (mm)	76	Number of rows	2
Drilling Pattern	Square	Delay (mm/s)	25
Initiation sequence	Square V	Charge length (m)	8
Burden (m)	2	Charge per hole (ANFO) (kg)	25
Spacing (m)	2.5	Total weight of charge (ANFO) (kg)	250
Bench Height (m)	9	Booster per hole (Pentolite) (kg)	0.5
Sub drilling (m)	1	Total weight of Booster (Pentolite) (kg)	5
Yield in volume ($\mathbf{m^3}$)	450	Yield in Ton	1260
Total weight of charge (ANFO+Pentolite) (kg)	255	Powder Factor ($\mathbf{kg/m^3}$)	0.56

Figure 5.5 Location of the test blast-2

5.6.3 Test Blast-3

On August 8, 2022, the third test blast was conducted. The blast happened on the 1st Bench at 4 p.m. Figure 5.6 shows that the blast had 15 holes that were angled 5° toward the face and designed to be drilled to a depth of 7 meters. The planned depth of the drill included a sub-drill of 1 meter, and the bench height was 6 meters. The planned burden was 2 meters, and the distance between holes was 2.20 meters. Most of the extra burden was put on the foot at the toe of the first row. Table 5.7 provides information about the bench face, blast design and profile. Figure 5.7 shows the location of test blast-3 on Google earth.

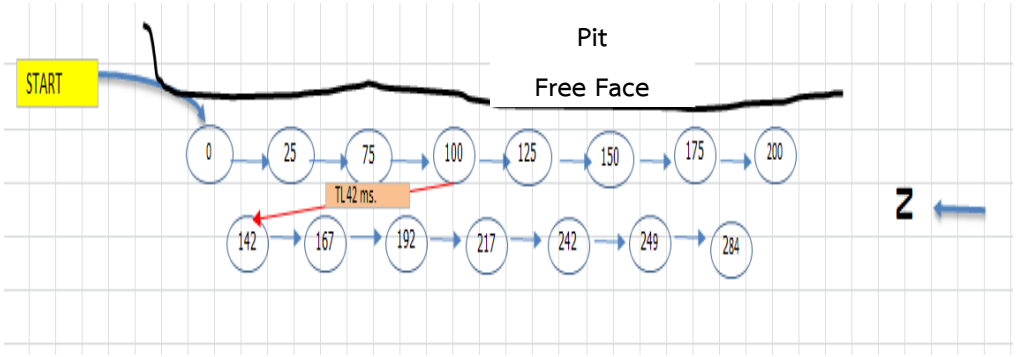

Figure 5.6 Drilling and initiation Pattern

Table 5.7 Dyno Nobel (rules of thumb) based blast design Parameters

Modified Design-2			
Parameter	**Value**	**Parameter**	**Value**
Rock Type	Pyrophyllite	Hole Depth (m)	7
UCS (MPa)	85 (Medium)	Stemming (m)	2
Density (g/cm^3)	2.8	Number of Holes	15
Borehole diameter (mm)	76	Number of rows	2
Drilling Pattern	Rectangular	Delay (mm/s)	25
Initiation sequence	Staggered	Charge length (m)	5
Burden (m)	2	Charge per hole (ANFO) (kg)	16
Spacing (m)	2.2	Total weight of charge (ANFO) (kg)	240
Bench Height (m)	6	Booster per hole (Pentolite) (kg)	1
Sub drilling (m)	1	Yield in volume (m^3)	396
Total weight of Booster (Pentolite) (kg)	15	Yield in Ton	1108
Total weight of charge (ANFO+Pentolite) (kg)	255	Powder Factor (kg/m^3)	0.64

Figure 5.7 Location of the test blast-3

5.6.4 Test Blast-4

On August 9, 2022, the third test blast was conducted. The blast happened on the 1st Bench at 4 p.m. Figure 5.8 shows that the blast had 15 holes that were angled 5° toward the face and designed to be drilled to a depth of 7 meters. The planned depth of the drill included a sub-drill of 1 meter, and the bench height was 6 meters. The planned burden was 2 meters, and the distance between holes was 2.20 meters. Most of the extra burden was put on the foot at the toe of the first row. Table 5.8 provides information about the bench face, blast design and profile. Figure 5.9 shows the location of test blast-3 on Google earth.

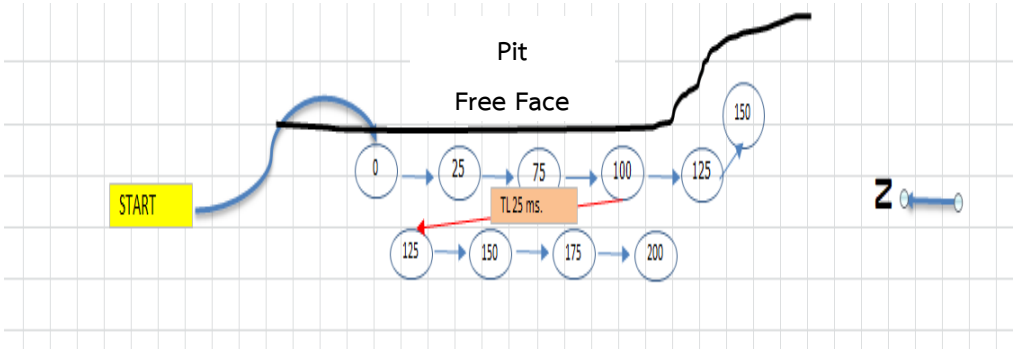

Figure 5.8 Drilling and Initiation Pattern

Table 5.8 Stig O Olofson (1989) blast design based parameters

Modified Design-3			
Parameter	**Value**	**Parameter**	**Value**
Rock Type	Pyrophyllite	Number of Holes	10
UCS (MPa)	85 (Medium)	Number of rows	2
Density $(\mathbf{g/cm^3})$	2.8	Delay (hole to hole) (mm/s)	25
Borehole diameter (mm)	76	Delay (Row to Row) (mm/s)	25
Drilling Pattern	Rectangular	Charge length (m)	5
Initiation sequence	Staggered	Charge per hole (ANFO) (kg)	16
Number or Rows	2	Total weight of charge (ANFO) (kg)	160
Burden (m)	2	Booster per hole (Pentolite) (kg)	0.5
Spacing (m)	2	Total weight of Booster (Pentolite) (kg)	5
Bench Height (m)	6	Total weight of charge (ANFO+Pentolite) (kg)	165
Sub drilling (m)	1	Yield in volume $(\mathbf{m^3})$	240
Hole Depth (m)	7	Blast in Ton	672
Stemming (m)	2	Powder Factor $(\mathbf{kg/m^3})$	0.68

Figure 5.9 Location of the test blast-4

5.6.5 Test Blast-5

On September 24, 2022, the fourth test blast was conducted. The blast happened on the 3rd Bench at 4 p.m. Figure 5.10 shows that the blast had 16 holes that were angled 5° toward the face and were meant to be drilled to a depth of 9–10 meters. The planned drill depth had a sub-drill of 1-2 meters, and the bench height was 8–9 meters. The burden was 2 meters, and the distance between holes was 2.5 meters. Most of the extra burden was put on the foot at the toe of the first row. Table 5.8 provides the blast design, bench face, and profile data. Figure 5.11 shows the location of the test blast 5 on Google earth.

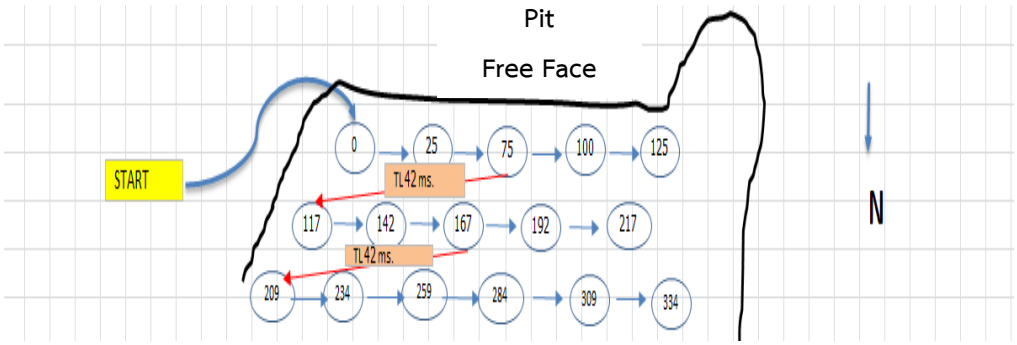

Figure 5.10 Drilling and initiation Pattern

Table 5.9 Hybrid Blast design model

Modified Design-4			
Parameter	**Value**	**Parameter**	**Value**
Rock Type	Pyrophyllite	Average Hole Depth (m)	9.5
UCS (MPa)	85 (Medium)	Stemming (m)	2
Density (g/cm^3)	2.8	Number of Holes	16
Borehole diameter (mm)	76	Number of rows	2
Drilling Pattern	Rectangular	Delay (hole to hole)(mm/s)	25
Initiation sequence	Staggered	Delay (Row to Row) (mm/s)	42
Burden (m)	2	Charge length (m)	7.5
Spacing (m)	2	Charge per hole (ANFO) (kg)	26
Maximum Bench Height (m)	9	Total weight of charge (ANFO) (kg)	416
Maximum Bench Height (m)	8	Booster per hole (Pentolite) (kg)	1
Average Bench Height (m)	8.5	Total weight of Booster (Pentolite) (kg)	16
Maximum Sub drilling (m)	2	Total weight of charge (ANFO+Pentolite) (kg)	432
Minimum Sub drilling (m)	1	Yield in volume (m^3)	680
Average Sub drilling (m)	1.5	Yield in Ton	1904
Maximum Hole Depth (m)	10	Powder Factor (kg/m^3)	0.63
Minimum Hole Depth (m)	9		

Figure 5.11 Location of the test blast-5

CHAPTER 6

RESULTS AND DISCUSSION

6.1 Introduction

This section presents the fragmentation analysis done through digital image analysis using image-J size distribution software and PPV evaluation done through the digital device using Instantel Micromate. PPV prediction results of all five blasts are also presented in this chapter. Furthermore, the results are discussed at the end of this chapter

6.2 Fragmentation Analysis

The result and discussion of fragmentation size distribution analysis are obtained through digital image analysis using ImageJ software. A total of 10 photos were taken after the blasts, which were then evaluated manually to ensure they were true and matched with the actual fragments. Muckpile profile of each blast can be found in the Appendix C.

The fragmentation size distribution histograms and curves for each blast are created to understand the size distribution, presented in Figures 6.2 to 6.6. Based on the performance of each blast, discussion and observations were made. Figure 6.1 shows the fragmentation analysis with a scale of 30 inches by imageJ software. Table 6.1 summarizes the fragmentation analysis results of the five test blasts conducted at Pyrophyllite Mine Saraburi, Thailand.

6.2.1 Test Blast-1

Figure 6.2 shows the size distribution of test blast-1 fragmentations. The results show that the average fragment size is 25 inches below the crusher gap of 30 inches. However, the fragment size counts show that the percentage of big fragments size greater than 30 inches is high, which can directly affect the downstream operations. This histogram indicates that the fragmentation is not good as the top-size material produced by the blast-1 percentage is still very high. There is a big difference between

the minimum and maximum fragment size, which is why it is tried to optimize the blasting design parameters to decrease this gap and produce fragmentation with minimum boulders.

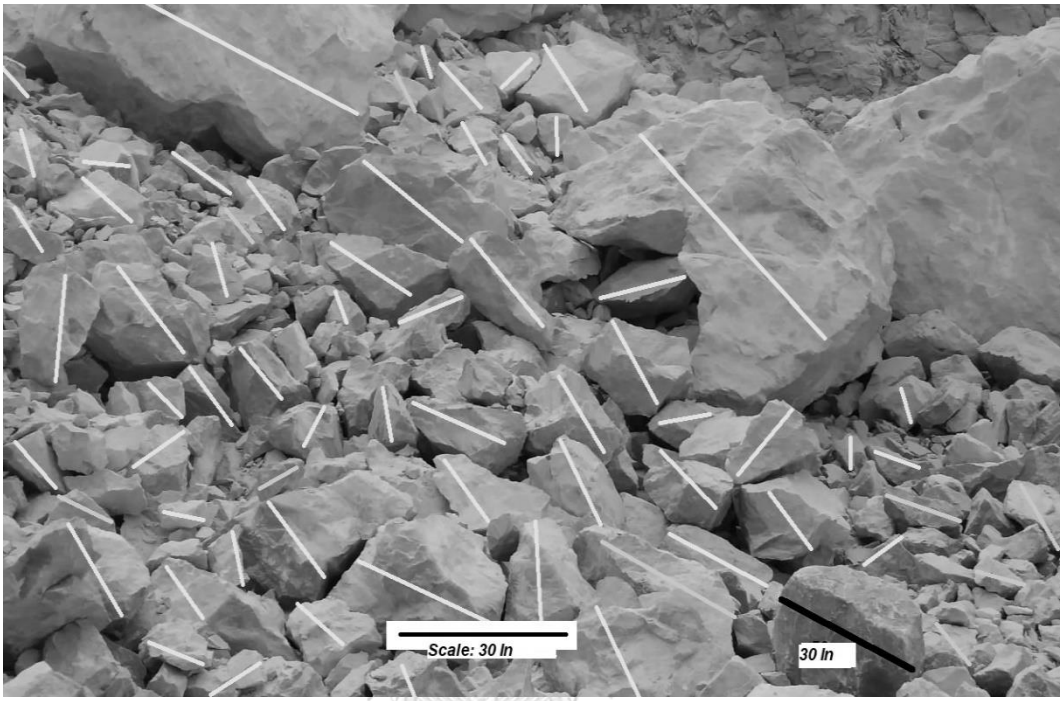

Figure 6.1 Muckpile digital analysis by ImageJ software

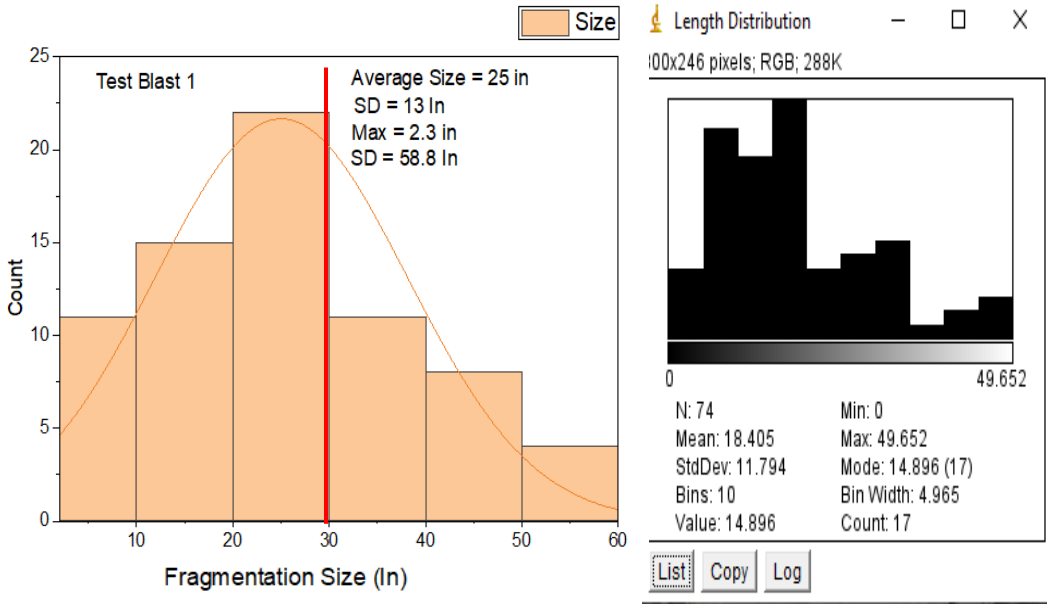

Figure 6.2 Average size distribution of the blast-1 muckpile

6.2.2 Test Blast-2

Figure 6.3 shows that the average size distribution of the fragments from test Blast-2 is 18 inches, which is lower than the crusher feed size. The results further explained that Modified design-1 produced fewer boulders than this quarry's conventional blast design. However, there is still a gap between minimum and maximum fragment size. The histogram indicates that the blast is good with fair fragmentation distribution.

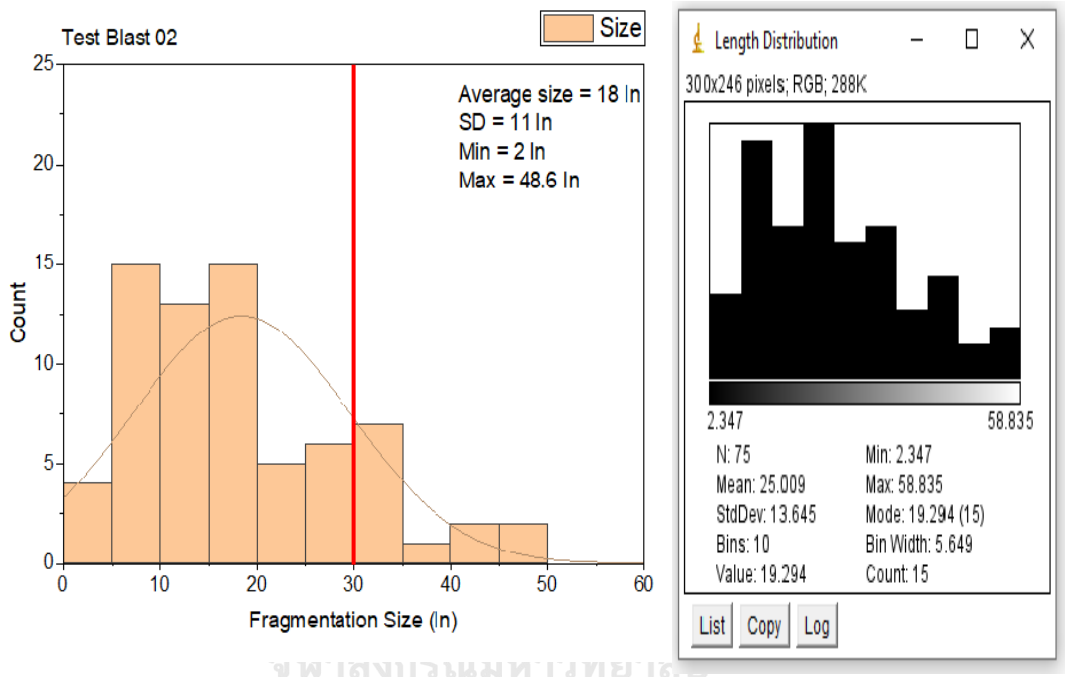

Figure 6.3 Average size distribution of the blast-2 muckpile

6.2.3 Test Blast-3

From Figure 6.4, the measured average fragmentation size was 20 inches, which is more than measured in Modified design 1. The measured average size is still under the crusher feed size, but the amount of boulders is noticeable. The histogram revealed that the Test Blast-3 is a good blast with less number of boulders production.

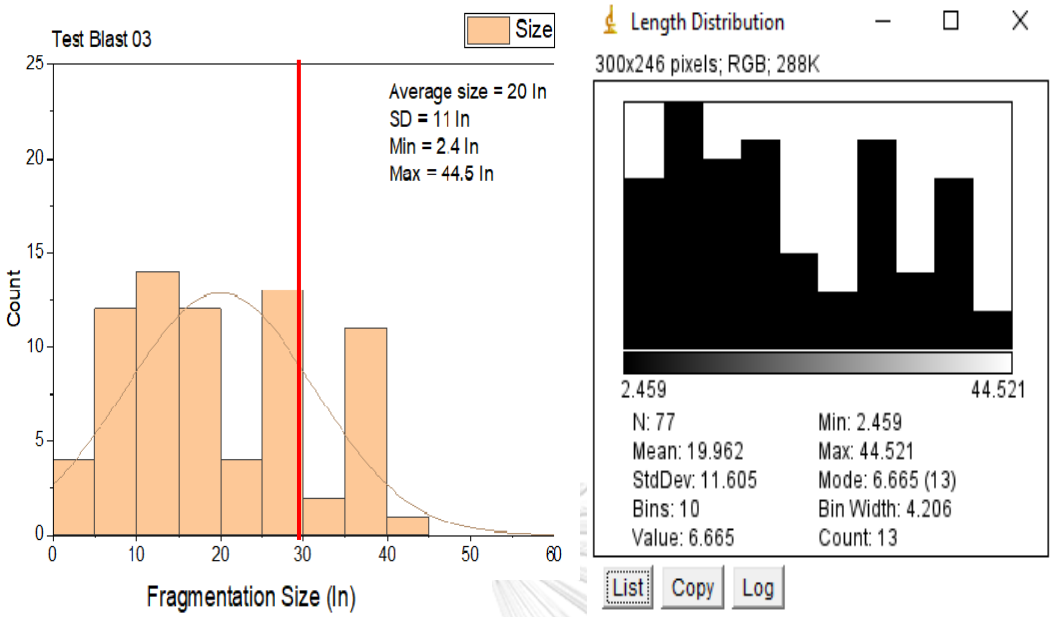

Figure 6.4 Average size distribution of the blast-3 muckpile

6.2.4 Test Blast-4

Figure 6.5 shows that the average fragmentation size of blasted material is 18 inches, which is more good than traditional, modified 1 and 2 designs. The gap between minimum and maximum fragments size is big, but the percentage count of boulders production is less. The histogram revealed that modified blast design-3 is good and gives optimum fragmentation size. The boulders produced from this blast are not big, and the pneumatic pick hammer can easily reduce the boulders into the required fragments.

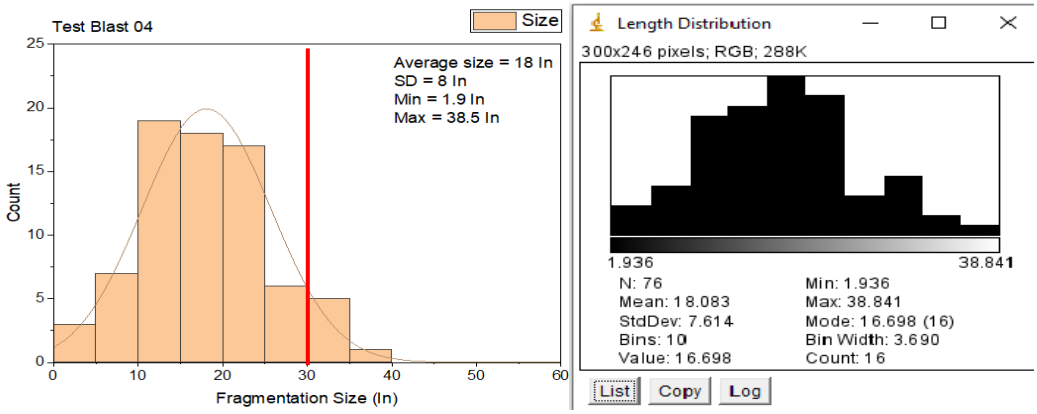

Figure 6.5 Average size distribution of the blast-4 muckpile

6.2.5 Test Blast-5

Figure 6.6 shows that more than 90 percent of the fragment size of the test blast-5 was less than 30 inches. The average fragmentation size is measured 14 inches which is more optimized than the rest of the blasts. The gap between the minimum and maximum fragments size is big but the count of maximum fragment is less, and the production of boulders is unnoticeable. The histogram indicates that blast-5 using modified blast design-4 was the best of all designs.

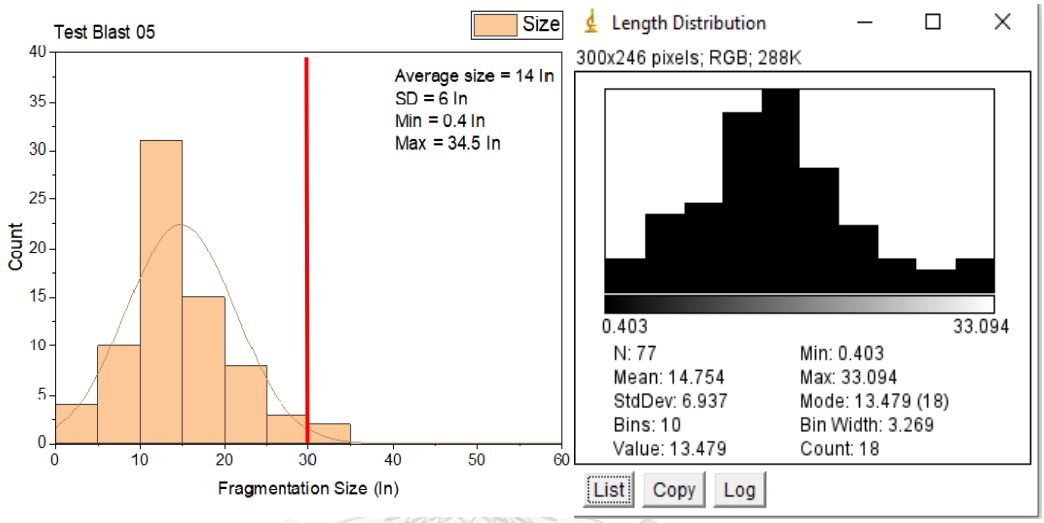

Figure 6.6 Average size distribution of the blast-5 muckpile

Table 6.1 Summary of the fragmentation analysis of the five blasts designs

Blast	Blast Design	Mean Area (in^2)	Max (in)	Min (in)	SD (in)	Average particle size (in)	Passing (≤30 in) %
1	Conventional Design	4.0	58.8	2.3	13	25	50
2	Modified Design-1	1.5	48.6	2.0	11	18	65
3	Modified Design-2	2.0	44.5	2.4	11	20	62
4	Modified Design-3	2.5	38.5	1.9	8	18	80
5	Modified Design-4	3.0	35.5	0.4	6	14	90

6.3 Fragmentation Analysis Results Comparisons

Different parameters of blast design are compared with image analysis results to understand the relationship.

6.3.1 Powder Factor - Average Size Relationship

Figure 6.7 shows that the fragments average size decreases with the powder factor. This indicates that Pyrophyllite rock mass is strong enough and needs more explosive energy.

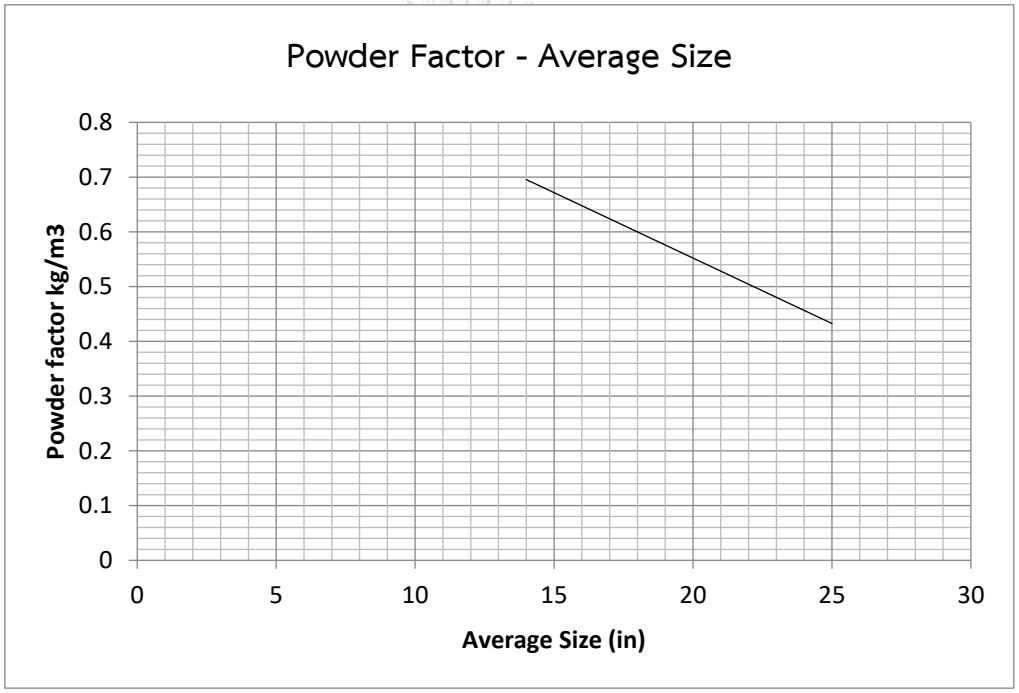

Figure 6.7 Relationship between Powder factor and average size (in)

6.3.2 Stiffness Ratio - Average Size Relationship

Figure 6.8 shows that the average fragment size decreased with an increasing stiffness ratio. The passing percentage of fragments increased between the stiffness ratio of 3 and 4.5, which cleared that the average size of fragments not only depends on burden but also on bench height.

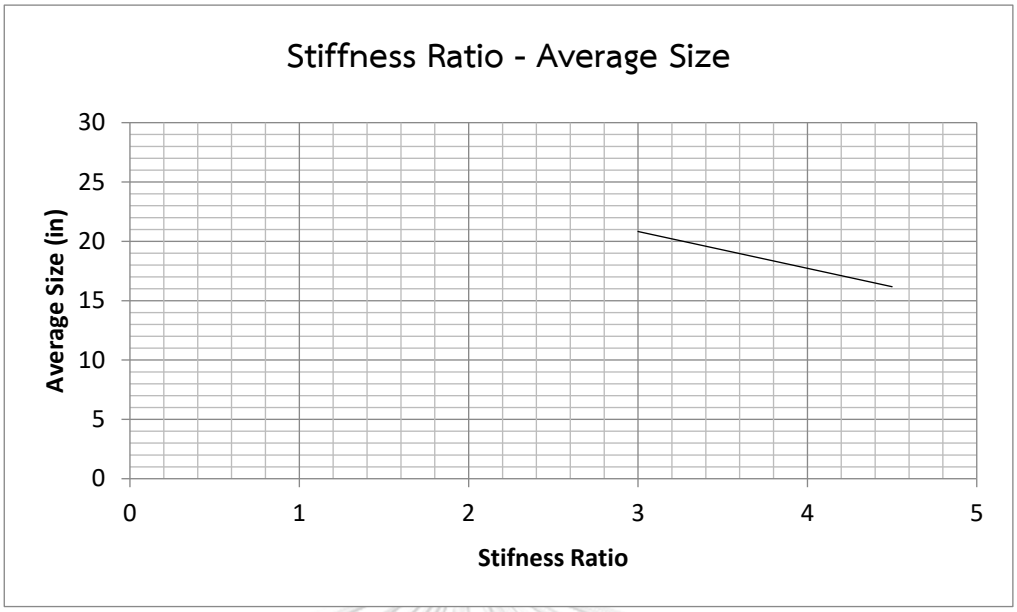

Figure 6.8 Relationship between stiffness ratio and average size (in)

6.3.3 Average Size - Row to Row Delay Relationship

Figure 6.9 shows that delay time between row to row affects the fragmentation size. 42 ms delays show good fragmentation performance as compared with 25 ms delays. The fragmentation shows optimal results when the row to row delay time is more than 25 ms.

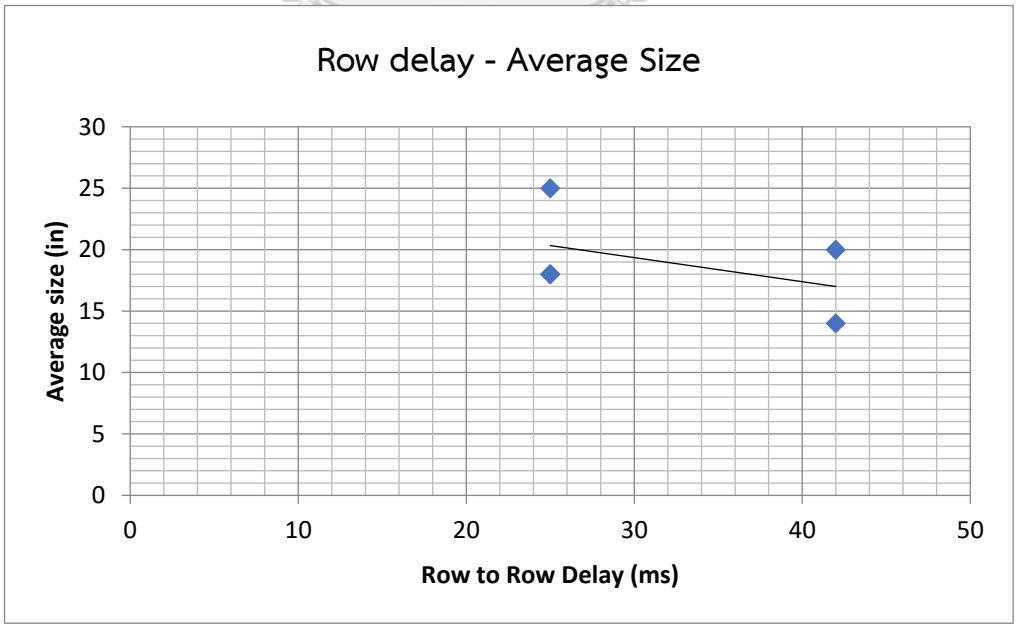

Figure 6.9 Relationship between Row to Row delay and average size (in)

6.4 Fragmentation Analysis Discussion

The fact is that optimal fragmentation size depends on the quarry or company requirements. Normally, those fragments can be called optimal if their size is less than the crusher's maximum feed size.

The required feed size of fragmentation at this quarry is ≤ 30 inches, but the current blasting design produces a fragmentation size greater than 30 inches. To ensure this, test blast-1 was conducted using a conventional blast design. It found that the average size distribution (imageJ) of test blast-1 was 25 inches, containing 50 percent of boulders and 50 percent of fragmentation size less than 30 inches.

To optimize the conventional blast design, Brazilian test, Uniaxial Compressive Strength, point load test, XRD, and XRF to find the rock mass parameters at the pyrophyllite quarry. After analyzing rock mass parameters results, four modified blasting designs were proposed (Table 5.6- Table 5.9). These designs were applied in the field to check the fragmentation results using ImageJ software.

Test Blast-2 was conducted using modified blast design-1, where the geometric parameters (burden, spacing, stemming, and sub-drill) were calculated based on the Uniaxial Compressive Strength of rock mass (UCS). After the blast, the size distribution histogram revealed that fragmentation performance had improved, and the passing percentage increased from 50 to 65. However, the boulders were still big enough for secondary blasting, which could disturb the downstream operations. Moreover, the average fragmentation size of the blast was measured 18 inches, which is lesser than the conventional blast design average size distribution.

Test Blast-3 was conducted using modified design-2, where the geometric parameters (burden, spacing, charge column, sub-drill, and stemming) were calculated using Dyno Nobel Pacific Limited 2020 blast design model. After the digital analysis of the muckpile (Figure 6.4), it is found that the average fragmentation size increased from 18 to 20 inches. The increase in the production of boulders was noticed because of

the joints in the strata. However, the performance of modified blast design-2 was good, with a passing fragmentation percentage of 62.

Test blast-4 was conducted using modified design-3. The geometric and explosive parameters were calculated based on Stig O Olofson's (1989) empirical models and formulas. The fragmentation analysis software results were very good, as the passing percentage was 80, with an average fragment size of 18 inches. Boulders production was decreased, and the performance of the fragmentation was improved. The size distribution histogram (Figure 6.5) indicated that modified blast design-3 was an excellent design matching the quarry condition.

Test Blast-5 was conducted using modified blast design-4. The geometric and explosive parameters were calculated using hybrid model. The size distribution histogram (Figure 6.6) shows that the average size distribution decreased to 14 inches with a 90 percent passing rate. The boulders' percentage decreased and can hardly be noticeable at the muck pile. This shows that considering mixed models for calculating geometric and explosive parameters is important during the blast design.

The comparison between powder factor and average distribution size (inches) in Figure 6.7 revealed that the average size of the distribution decreased with the increase of powder factor. Powder factor increase with the strength of the rock. The geotechnical properties and geology of the benches at this quarry are different, so powder factor values vary from 0.37 to 0.68 kg/m3. Furthermore, powder factor values also indicated that the cost per blast is also not the same, and it also varies with the strength and geology of the quarry, as blast on bench#2 (hard rock) may need more explosive to blast than bench#3 at pyrophyllite Mine Saraburi, Thailand.

Stiffness is the burden-to-height ratio. It gives us an idea of the fragmentation before the blast. Figure 6.8 shows the stiffness ratio and our measured fragmentation average size going on the same tract; as the stiffness ratio increase from 3 to 4.5, the average fragmentation size decrease with it. It means that the predictive fragmentation

ratio and actual measured values are the same, indicating that our modified blast designs are well-suitable for the quarry condition.

Delay plays an important role during blasting, and our initiation system must have a hole-to-hole and Row to Row delays. Figure 6.9 shows the relationship between Row to Row delay and average size. It is understood from the Figure 6.9 plot that 42 milliseconds delays between row to row initiation system is optimal as it gives minimum average size compared with 25-millisecond delays. As there is a variation of geology in the pyrophyllite quarry, the drilling patterns are adopted according to the conditions of the face and bench.

6.5 Ground Vibration Analysis

In order to predict the PPV, ground vibrations were measured for 5 test blasts at two different points (crusher and mine office). The Instantel Micromate seismograph device was used to monitor and record the blast-induced ground vibrations. The portable GPS device measured the distance between the blasting site and the monitoring station. Charge weight per hole and maximum charge per delay were recorded for each shot throughout the field investigation. Table 5.5 to 5.9 shows the design parameters for each blast with measured results. ANFO as a blasting agent, pentolite as a booster, and a non-electric (NONEL) delay system were used for each blast in order to initiate the charge. The timing patterns between rows differed for each blast; however, a 25 ms delay system was used between holes. The prediction Equations (6.1) and (6.2) Proposed by USBM were used to determine scaled distance and the PPV. Table 6.2 summarizes the vibrations recorded near the blasting site at pyrophyllite mine Saraburi, Thailand.

$$\text{Scaled Distance (SD)} = \frac{D}{\sqrt{Q}} \qquad \text{Equation (6.1)}$$

$$PPV = K\left(\frac{D}{Q^{0.5}}\right)^{-1.6} \qquad \text{Equation (6.2)}$$

Where:

D= Distance from blasting site (m)

Q = Maximum charge (kg)

K = Site and rock constant

Table 6.2 Summary of the recorded ground vibrations

Blast	Design	Bench	Max Charge per delay (Q) (kg)	Distance (D) (m)	Scaled Distance (SD) ($m/kg^{0.5}$)	Peak Particle Velocity (PPV) (mm/s)
1	Conventional	3	22.5	350	73.78	1.16
2	Modified-1	3	25.5	300	59.40	1.65
3	Modified-2	1	17.0	250	60.63	1.60
4	Modified-3	1	16.5	400	98.47	0.73
5	Modified-4	3	27.0	350	67.35	1.35

The shortest distance between the blasting site and near structures is 400 meters. That is why each blast was monitored at a different distance (250 to 350 meters) from the blasting site to examine the vibration more precisely. The highest peak particle velocity was recorded inside the quarry area as 1.65 mm/s near the main crusher at 300m away from the test blast-2 (Modified design-1). The lowest PPV was also recorded inside the quarry area as 0.73 mm/s near the mine office at 400m away from the test blast-4, using modified design-4.

6.5.1 PPV - Scaled Distance Relationship

Figure 6.10 revealed the relationship between PPV and scaled distance. The PPV of the pyrophyllite decrease with the increase of scaled distance and vice versa. The PPV and scaled distance relationship further shows the scattering of data which might be possible because of the time interval between rows, geological conditions, initiation system, design parameters, and charge per hole. R-Squared value of 0.96 indicates that the regression analysis explains 96% of the variance of the PPV. Although, the correlation was found 98% between PPV and scaled distance.

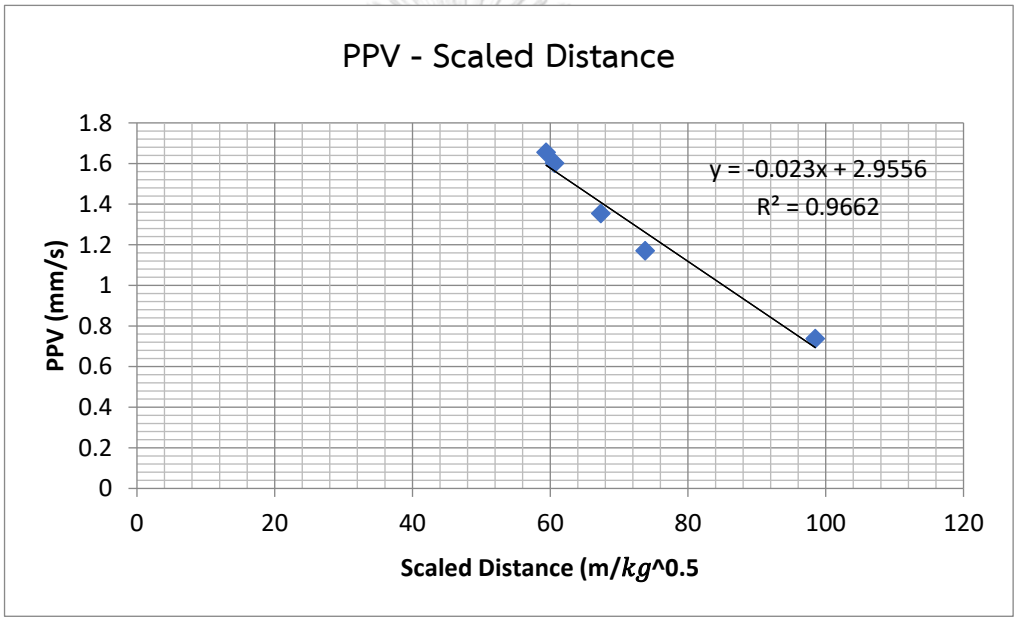

Figure 6.10 Plot of PPV versus Scaled distance

6.6 Ground Vibration Analysis Discussion

The ground vibration data collected for five test blasts throughout the field investigations are shown in Table 6.2. According to the USBM standard, the measured PPV at the pyrophyllite mine was insufficient to damage any nearby structure. The measured PPV varies from 0.73 to 1.65 mm/s, indicating that the blast-induced vibrations intensities were not high but bearable under the safety limit. Therefore, the blasting operations using the modified designs were very safe, and it will be unlikely if the PPV in such a range can affect any structure in the vicinity of the mine.

Correspondingly, structures in the vicinity of the blasting site are experiencing very low ground vibrations that will not damage or affect any old, new, or concrete structure. Due to this reason, it can be concluded that the proposed blasting designs with optimized parameters were optimal, safe, and matched the geology of the site.

The highest measured PPV was 1.65 mm/s, which is very less than the standard PPV of 25 mm/s recommended by USBM and the Department of Primary Industries and Mines (DPIM, Thailand). It was also observed that ground vibrations were very low and did not trigger the ground vibration instruments to record the PPV.

The PPV-Scaled distance relationship shown in Figure 6.10 reveals that the value of PPV decreases with increasing scaled distance. PPV also has a direct relationship with the distance between the blasting site and monitoring station, as the values of PPV decrease as the distance between increases shown in Figure 6.10.

Table 6.2 indicates that the amount of explosive used per delay also affects the ground vibration intensity in terms of PPV. The values of PPV were high for blast-2 and 4, as the amount used per delay was 25.5 kg and 27 kg. However, the highest peak particle velocity (PPV) value is still within the standard, and there is no threat or impact on the environment in the vicinity of the blasting site.

There is variation in the plotted graph of PPV and scaled distance, and this could be because of the geological condition, water condition, initiations system, maximum charge per hole, blasting site to monitoring station distance, hole to hole, and row to row delay system and the calculated parameters of blasting designs.

The results also concluded that it is safe to use the proposed modeled blasting designs (1-4) at the pyrophyllite mine, as the value of PPV is less than 2 mm/s, which cannot affect the environment or annoy the nearby humans directly. This is why the proposed designs were recommended to the pyrophyllite mine in Saraburi province, Thailand.

CHAPTER 7

CONCLUSIONS AND RECOMMENDATION

7.1 Conclusions

Five test blasts were examined in this study to investigate the optimal blast design parameters for producing good fragmentation according to the size of the crusher feeder and to control blast-induced ground vibrations at a Khao Mai Nuan Pyrophyllite quarry, Saraburi Province, Thailand. ImageJ, a digital analysis software, was employed to analyze the muckpiles resulting from the test blasts. Finally, the average size distribution of the fragments and curves for each blast muckpile were constructed based on the data from image analysis. The data were then visualized with the help of origon 2022b software. For the ground vibration (PPV) prediction, Langefors & Kihlstrom 1973, Scaled distance predictive empirical equations were used. In addition, the Instantel Micromate seismograph device was used throughout the field investigations to measure PPV.

From the preceding experiments, results, analysis, and explanations, it can be clearly drawn that:

1) Fragmentation

a) The first test blast was based on an existing blast design, and the other four were modified according to pyrophyllite rock parameters and geological variation in the quarry. The modified blast designs based on Uniaxial Compressive Strength (UCS), Dyno Nobel Pacific Pty Limited 2020, and Stig O. Olofson (1989) models resulted in good fragmentation. This indicated that our proposed blast designs were well-suited for the quarry conditions.

b) Among the blasts conducted during field investigations, the lowest average fragment size was measured 14 inches using hybrid modified blast design-4,

which had the most optimized average value compared to the other blast designs.

c) The second most optimized average fragment was measured 18 inches using Stig O Olofson (1989) blasting model.

d) Short and long delays play an important role in muckpile size distribution. Figure 6.9 shows that the short delay system does not improve the fragmentation performance in a pyrophyllite quarry. The optimal average size was measured using a long delay system. The 25 ms delay time had poor fragmentation with a 50% passing rate; however, the 42 ms delay time produced good fragmentation. This showed that the average fragments size changed with increasing delay time.

e) The effects of a specific charge and geometry on the average size of fragmentation were analyzed for each tested blast. Figure 6.7 shows that the average fragmentation size decreased with an increasing specific charge while the passing percentage of the fragments increased. Hence, decreeing spacing and burden in blast design can help increase the fragments' uniformity.

f) Drilling patterns with respect to the current geological condition of the pyrophyllite quarry were also discussed in this study. The drilling pattern for each test blast was adopted according to the conditions of the face and bench, as there is geological variation among quarry benches.

2) Ground Vibration (PPV)

a) All results from measurement demonstrated that blast-induced ground vibrations generated and propagated at the area were very low to cause any kind of damage to any nearby structures within the vicinity of the mine.

b) The highest peak particle velocity (PPV) recorded at a distance of 300 m away from the blasting site was 1.65 mm/s, while the lowest peak particle velocity (PPV) recorded at a distance of 400 m away from the blasting site was 0.37

mm/s. Therefore, it can be concluded that all the modified designs used for test blasts were optimized and environmental friendly designs, with no high-level blast-induced ground vibrations, and it will be very unlikely if the PPV in such a range can affect any structure in the vicinity of the mine.

c) All the recorded peak particle velocities (PPV) from tested blast were within the safe limit standards set by the United State Bureau of Mine (USBM), German Vibration Standards (DIN 4150), and Department of Primary Industries and Mines (DPIM, Thailand), which is 25 mm/s.

d) There was a variation in the plotted graph of Peak Particle Velocity (PPV) and Scale Distance (SD), and this could be because Peak Particle Velocity (PPV) depends on geological conditions, vibration frequency, scaled distance, joints, faults, layers, water conditions, initiation systems, blast design parameters like burden space, and explosive per delay. Hence, it is necessary to establish a specific empirical equation for the predictions of PPV based on the site conditions and constant.

e) An appropriate guideline is necessary for the control blasting operations at the Khao Mai Nuan pyrophyllite mine regarding environmental, safety, technical and economic attributes. That is why these modified tested blast designs were recommended to the management of the pyrophyllite quarry.

7.2 Recommendation

Khao Mai Nuan Pyrophyllite Mine is a small-scale mining operation site, producing around 1500 tons of material per month. A total of five experiments were conducted throughout the field investigations, in which each blast was carried out using a different blast design. Blasting operations are not that often on this site, and that's why a lower number of experiments were carried out to conduct this study.

The aspects that need attention from future researchers are:

a) The research work done in this study is based on a specific site of Pyrophyllite. Hence, it can be further expanded to other quarries with different rock characteristics and types in order to check the validity of the proposed modified blast designs.
b) Increasing the number of experiments using the proposed modified blast designs will improve performance and decrease variation in the data.
c) Further geological investigation is necessary at the Khao Mai Nuan pyrophyllite quarry to understand the geological setting of pyrophyllite.
d) More digital photos should be taken for the image analysis to decrease the variation in the plotted data and increase the level of confidence.
e) Future studies should employ Split-Desktop or Wip Frag for size distribution analysis, as these softwares generates more precise results than imageJ.

REFERENCES

[1] Tomberg, T., & Toomik, A. (1999). ENVIRONMENTAL IMPACT OF MINE BLASTING. Environment. Technology. Resources. Proceedings of the International Scientific and Practical Conference, 1, 213. https://doi.org/10.17770/etr1999vol1.1872

[2] Khademian, A., & Bagherpour, R. (2017). Environmentally sustainable mining through proper selection of explosives in blasting operation. Environmental Earth Sciences, 76(4), 166. https://doi.org/10.1007/s12665-017-6483-2

[3] Hidayat, S. (2021). Environmental Impacts of Open Pit Mining Blasting: Particular Discussions on Some Specific Issues. 1(1), 11.

[4] Marilena, Dario, & Pierpaolo. (2019). Analysis of predictor equations for determining the blast-induced vibration in rock blasting. International Journal of Mining Science and Technology, 29(6), 905–915.

[5] Mohamed, A. M. E., & Mohamed, A. E.-E. A. (2013). Quarry blasts assessment and their environmental impacts on the nearby oil pipelines, southeast of Helwan City, Egypt. NRIAG Journal of Astronomy and Geophysics, 2(1), 102–115. https://doi.org/10.1016/j.nrjag.2013.06.013

[6] Raina, A. K., Haldar, A., Chakraborty, A. K., Choudhury, P. B., Ramulu, M., & Bandyopadhyay, C. (2004). Human response to blast-induced vibration and air-overpressure: An Indian scenario. Bulletin of Engineering Geology and the Environment, 63(3), 209–214. https://doi.org/10.1007/s10064-004-0228-7

[7] Kecojevic, V., & Radomsky, M. (2004). The causes and control of loader- and truck-related fatalities in surface mining operations. Injury Control and Safety Promotion, 11(4), 239–251. https://doi.org/10.1080/156609704/233/289779

[8] Devine, J.F., 1966. Effect of charge weight on vibration levels from quarry blasting. USBM Report of Invest 6774.

[9] Elseman, I.A., 2000. Measurement and analysis of the effect of ground vibrations induced by blasting at the limestone quarries of the Egyptian cement company. ICEHM2000, Cairo University, Egypt, pp. 54–71.

[10]Tripathy, G. R., Shirke, R. R., & Kudale, M. D. (2016). Safety of engineered structures against blast vibrations: A case study. Journal of Rock Mechanics and Geotechnical Engineering, 8(2), 248–25

[11]Nicholson, R.F., 2005. Determination of blast vibrations using peak particle velocity at Bengal quarry. In: St. Ann, Jamaica. M.Sc. Thesis. Department of Civil and Environmental Engineering. Division of Rock Engineering.

[12]Khaled, M., Abdel Rahman, K., Bagy, E., 2007b. Safe blasting near the historical caves of, Tourah, Cairo, Egypt. In: Proceeding of the 4th EFEE World Conference on Explosives and Blasting, Vienna, Austria, p. 365.

[13]Nicholson, R.F., 2005. Determination of blast vibrations using peak particle velocity at Bengal quarry. In: St. Ann, Jamaica. M.Sc. Thesis. Department of Civil and Environmental Engineering. Division of Rock Engineering.

[14]Aksoy, M., Ak, H., & Konuk, A. (2019). Development of a Preliminary Blasting Design and Assessment of Environmental Impacts for a Quarry. Çukurova Üniversitesi Mühendislik-Mimarlık Fakültesi Dergisi, 34(2), 241–248.

[15]Nateghi, R. (2011). Prediction of ground vibration level induced by blasting at different rock units. International Journal of Rock Mechanics and Mining Sciences, 48(6), 899–908. https://doi.org/10.1016/j.ijrmms.2011.04.014

[16]Marto, A., Hajihassani, M., Armaghani, D. J., Mohamad, E. T., & Makhtar, A. M. (2014). A novel approach for blast-induced flyrock prediction based on imperialist competitive algorithm and artificial neural network. TheScientificWorldJournal, 2014, 643715. https://doi.org/10.1155/2014/643715

[17]Dhekne, P.Y. 2015. Environmental Impacts of Rock Blasting and Their Mitigation. International Journal of Chemical, Environmental & Biological Sciences, vol. 3, no. 1. pp. 46–50

[18]Coalfield ltd, n. (2016, July 1). Controlling Adverse Environmental Effects Of Blasting Operations Using Information Technology.

[19]Olofsson, stig o. (1988). 9789179706340: Applied explosives technology for construction and mining—AbeBooks—Stig O Olofsson: 9179706347.

[20]Kumar, R., Choudhury, D., & Bhargava, K. (2016). Determination of blast-induced ground vibration equations for rocks using mechanical and geological properties. Journal of Rock Mechanics and Geotechnical Engineering, 8(3), 341–349. https://doi.org/10.1016/j.jrmge.2015.10.009

[21]Nguyen, H., Bui, X.-N., Tran, Q.-H., & Moayedi, H. (2019). Predicting blast-induced peak particle velocity using BGAMs, ANN and SVM: A case study at the Nui Beo open-pit coal mine in Vietnam. Environmental Earth Sciences, 78(15), 479. https://doi.org/10.1007/s12665-019-8491-x

[22]Zeng, J., Roussis, P. C., Mohammed, A. S., Maraveas, C., Fatemi, S. A., Armaghani, D. J., & Asteris, P. G. (2021). Prediction of Peak Particle Velocity Caused by Blasting through the Combinations of Boosted-CHAID and SVM Models with Various Kernels. Applied Sciences, 11(8), 3705. https://doi.org/10.3390/app11083705

[23]Shadabfar, M., Gokdemir, C., Zhou, M., Kordestani, H., & Muho, E. V. (2020). Estimation of Damage Induced by Single-Hole Rock Blasting: A Review on Analytical, Numerical, and Experimental Solutions. Energies, 14(1), 29.

[24]Kuzu, C. (2008). The importance of site-specific characters in prediction models for blast-induced ground vibrations. Soil Dynamics and Earthquake Engineering, 28(5), 405–414. https://doi.org/10.1016/j.soildyn.2007.06.013

[25]Simangunsong, G. M., & Wahyudi, S. (2015). Effect of bedding plane on prediction blast-induced ground vibration in open pit coal mines. International Journal of Rock Mechanics and Mining Sciences, 79, 1–8.

[26]Cospedal Pérez-Cosío, J. de. (2019). Utilización de la medida de vibraciones en voladuras para el conocimiento de los daños al macizo de roca ornamental.

[27]Ak, H., & Konuk, A. (2008). The effect of discontinuity frequency on ground vibrations produced from bench blasting: A case study. Soil Dynamics and Earthquake Engineering, 28(9), 686–694.

[28]Iphar, M., Yavuz, M., & Ak, H. (2008). Prediction of ground vibrations resulting from the blasting operations in an open-pit mine by adaptive neuro-fuzzy inference system. Environmental Geology, 56(1), 97–107.

[29]Langefors U, Kihlstrom B (1963) The modern techniques of rock blasting. Wiley, New York

[30]Khandelwal M, Singh T (2007) Evaluation of blast-induced ground vibration predictors. Soil Dyn Earthq Eng 27:116–125

[31]Monjezi, M., Rezaei, M., & Yazdian, A. (2010). Prediction of backbreak in open-pit blasting using fuzzy set theory. Expert Systems with Applications, 37(3), 2637–2643. https://doi.org/10.1016/j.eswa.2009.08.014

[32]Hasanipanah, M., Jahed Armaghani, D., Khamesi, H., Bakhshandeh Amnieh, H., & Ghoraba, S. (2016). Several non-linear models in estimating air-overpressure resulting from mine blasting. Engineering with Computers, 32(3), 441–455. https://doi.org/10.1007/s00366-015-0425-y

[33]Liu, K., & Qiu, J. (2020). Investigation of Burn Cut Parameters and Model for One-Step Raise Excavation Based on Damage Evolution Mechanisms. Geofluids, 2020, e8879477. https://doi.org/10.1155/2020/8879477

[34]Yuan, P., Xu, Y., & Zheng, Z. (2017). Time-frequency analyses of blasting vibration signals in single-hole blasting model experiments. Journal of Vibroengineering, 19(1), 363–375. https://doi.org/10.21595/jve.2016.17031

[35]Ghosh A, Daemen JJ (1983) A simple new blast vibration predictor (based on wave propagation laws). The 24th US Symposium on Rock Mechanics (USRMS). American Rock Mechanics Association.

[36]Lundborg N, Persson A, Ladegaard-Pedersen A, Holmberg R(1975) Keeping the lid on flyrock in open-pit blasting. Eng Min J176:95–100

[37]Workman, J.L. & Calder, P.N. 1994. Flyrock prediction and control in surface mine Blasting. Proc. 20th Conf.on Explosives and Blasting Technique, Austin, Texas,30 January–3 February. Cleveland, OH: International Society of Explosives Engineers, pp. 59–74

[38]Schneider, L.C. 1996. Flyrock Part 1: Safety and causes,J. of Explosives Engineering 13(9): 18–20

[39]Maerz, N.H. & Palangio, T.W. (2004). Post-muckpile, pre-primary crusher, automated optical blast fragmentation sizing. Fragblast, 8(2), 119–136.

[40]Sudhakar, J., Adhikari, G.R. & Gupta, R.N. (2006). Comparison of fragmentation measurements by photographic and image analysis techniques. Rock Mechanics and Rock Engineering, 39 (2), 159-168.

[41]Siddiqui, F.I., Ali Shah, S.M. & Behan, M.Y. (2009). Measurement of size distribution of blasted rock using digital image processing. Engineering Science, 20(2), 81-93.

[42]Singh, A., Scoble, M., Lizotte, Y. & Crowther, G. (1991). Characterization of underground rock fragmentation. Geotechnical and Geological Engineering, 9(2), 93-107.

[43]Chakraborty, A.K., Raina, A.K., Ramulu, M., Choudhury, P.B., Haldar, A., Sahu, P. & Bandopadhyay, C. (2004). Parametric study to develop guidelines for blast fragmentation improvement in jointed and massive formations. Engineering Geology, 73(1-2), 105– 116.

[44]Mohammadnejad, M., Gholami, R., Sereshki, F. & Jamshidi, A. (2013). A new methodology to predict backbreak in blasting operation, International journal of rock mechanics and mining sciences, 60, 75-81

[45]Maerz, N.H., Palangio, T.C. & Franklin, J.A. (1996). WipFrag image based granulometry system. Proceedings of the FRAGBLAST 5 Workshop on Measurement of Blast Fragmentation, Montreal, Quebec, Canada, 91-99.

[46]Lopez Jimeno, Carlos, (1995). Drilling and blasting of rocks, Rotterdam A.A. Balkema

[47]Jemwa, G.T. & Aldrich, C. (2012). Estimating size fraction categories of coal particles on conveyor belts using image texture modeling methods. Expert Systems with Applications, 39(9), 7947–7960

[48]Zelin, Z., Jianguo, Y., Lihua, D. & Yuemin, Z. (2012). Estimation of coal particle size distribution by image segmentation. International Journal of Mining Science and Technology, 22, 739–744

[49]Evans, B.W.; Guggenheim, S. Talc, Pyrophyllite, and Related Minerals. In Hydrous Phyllosilicates; Bailey, S.W., Ed.; De Gruyter: Berlin, Germany, 2018.

[50]Harben, P.W. The Industrial Minerals Handybook: A Guide to Markets, Specifications and Prices, 4th ed.; Industrial Minerals Information: Surrey, UK, 2002; ISBN 1904333044.

Appendix A

Pre and Post Samples Visuals from UCS

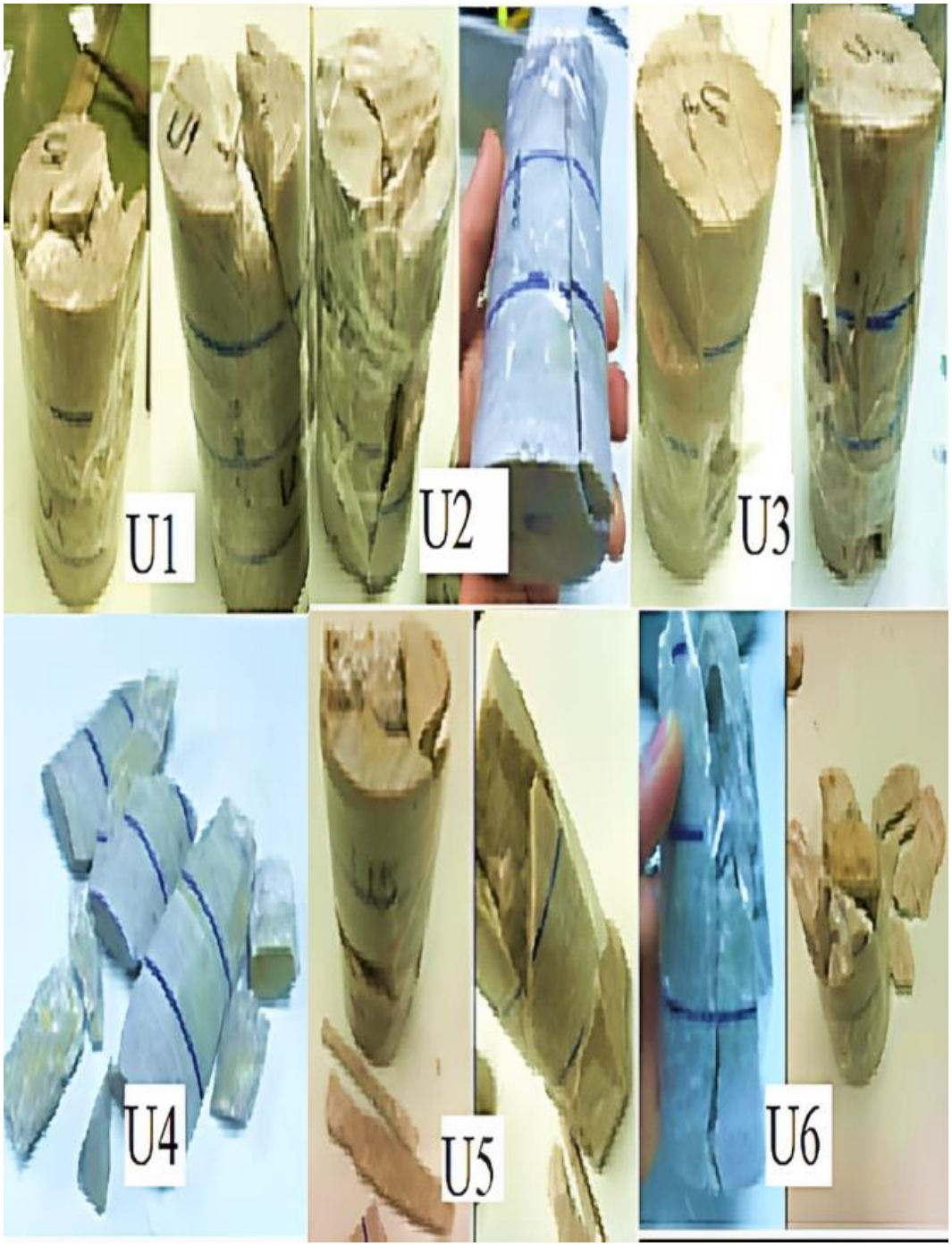

Appendix B

Pre and Post Samples Visuals from Brazilian Test

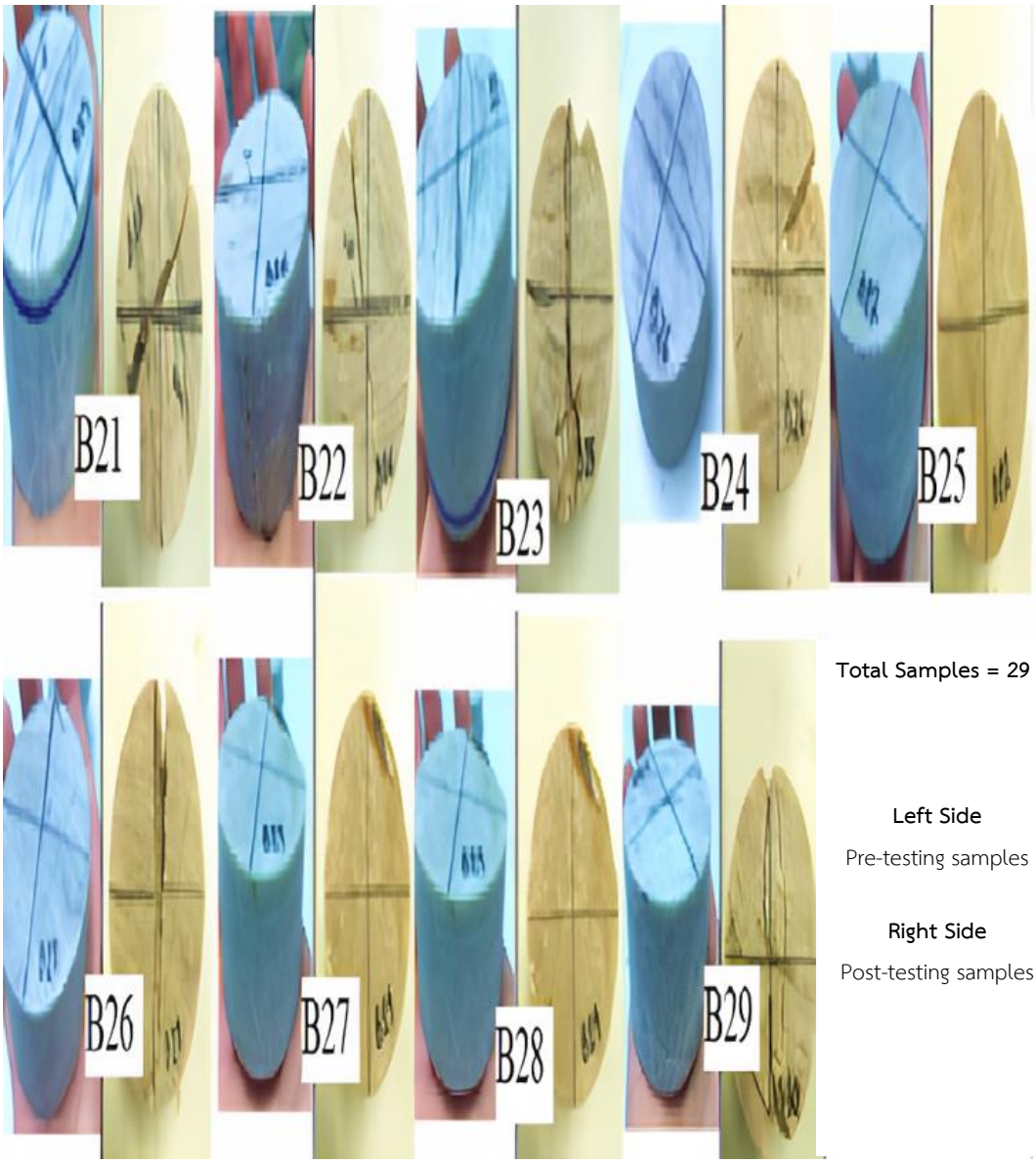
B21
B22
B23
B24
B25
B26
B27
B28
B29
Total Samples = 29
Left Side
Pre-testing samples
Right Side
Post-testing samples

Appendix C

Test blasts Muckpiles

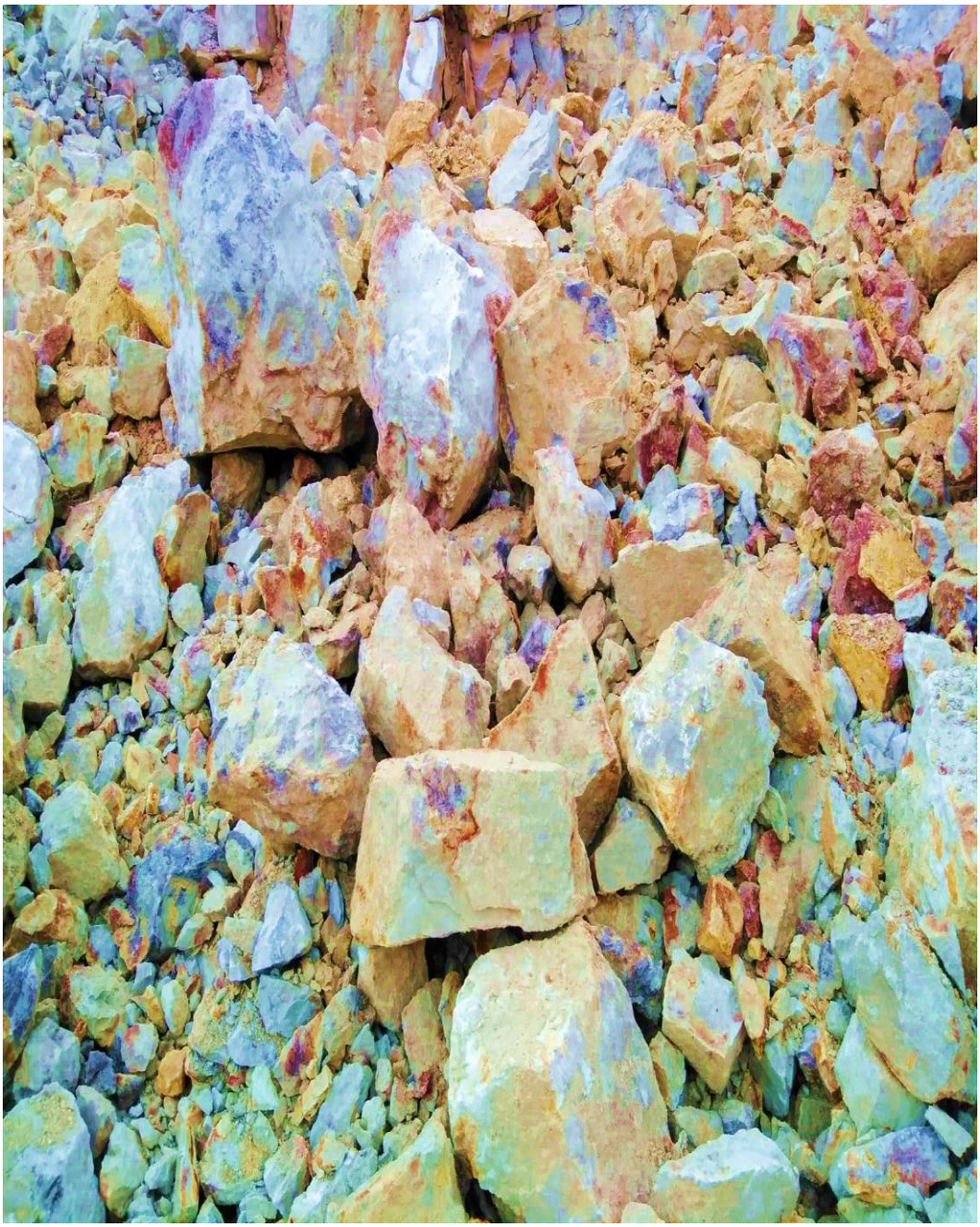

VITA

NAME	Arif khan
DATE OF BIRTH	03 February 1994
PLACE OF BIRTH	Swat, Pakistan
INSTITUTIONS ATTENDED	University of Engineering & Technology, Peshawar, Pakistan
HOME ADDRESS	Village: Manglor, City: Mingora, District: Swat, Province: KPK, Pakistan
PUBLICATION	NA
AWARD RECEIVED	NA